Bioactive Materials 20 (2023) 286–305

Contents lists available at ScienceDirect

Bioactive Materials

journal homepage: www.keaipublishing.com/en/journals/bioactive-materials

Maturation of induced pluripotent stem cell-derived cardiomyocytes and its therapeutic effect on myocardial infarction in mouse

Peng Wu [a,b,1], Xiyalatu Sai [a,b,1], Zhetao Li [a,b,1], Xing Ye [a,b,1], Li Jin [d], Guihuan Liu [e], Ge Li [b,c], Pingzhen Yang [d], Mingyi Zhao [b,c,****], Shuoji Zhu [b,c,***], Nanbo Liu [b,c,**], Ping Zhu [a,b,c,*]

[a] The Second School of Clinical Medicine, Southern Medical University, Guangzhou, 510515, China
[b] Department of Cardiac Surgery, Guangdong Cardiovascular Institute, Guangdong Provincial People's Hospital, Guangdong Academy of Medical Sciences, Guangzhou, 510100, China
[c] Guangdong Provincial Key Laboratory of Pathogenesis, Targeted Prevention and Treatment of Heart Disease, Guangzhou, 510100, China
[d] Zhujiang Hospital, Southern Medical University, Guangzhou, 510280, China
[e] Guangdong Cardiovascular Institute, Guangdong Provincial People's Hospital, Guangdong Academy of Medical Sciences, School of Medicine, South China University of Technology, Guangzhou, 510080, China

ARTICLE INFO

Keywords:
Induced pluripotent stem cell
Cardiomyocytes
Mature
Myocardial infarction treatment

ABSTRACT

Induced pluripotent stem cell-derived cardiomyocytes (iPSC-CMs) have an irreplaceable role in the treatment of myocardial infarction (MI), which can be injected into the transplanted area with new cardiomyocytes (Cardiomyocytes, CMs), and improve myocardial function. However, the immaturity of the structure and function of iPSC-CMs is the main bottleneck at present. Since collagen participates in the formation of extracellular matrix (ECM), we synthesized nano colloidal gelatin (Gel) with collagen as the main component, and confirmed that the biomaterial has good biocompatibility and is suitable for cellular in vitro growth. Subsequently, we combined the PI3K/AKT/mTOR pathway inhibitor BEZ-235 with Gel and found that the two combined increased the sarcomere length and action potential amplitude (APA) of iPSC-CMs, and improved the Ca^{2+} processing ability, the maturation of mitochondrial morphological structure and metabolic function. Not only that, Gel can also prolong the retention rate of iPSC-CMs in the myocardium and increase the expression of Cx43 and angiogenesis in the transplanted area of mature iPSC-CMs, which also provides a reliable basis for the subsequent treatment of mature iPSC-CMs.

1. Introduction

At present, the prevalence of cardiovascular disease in China is still rising, and the mortality rate has remained at a high level. Despite significant advances in therapies such as drugs and surgery, extensive and irreversible loss of cardiomyocytes (CMs) due to severe ischemia cannot be avoided. Because adult CMs cannot regenerate, the repair of ischemic myocardium lacks an effective source of CMs. Recently, many studies have pointed out that stem cells can repair damaged myocardium to improve cardiac function, but most of their effects depend on paracrine function, and their ability to differentiate into CMs is weak, and cannot effectively provide new CMs for ischemic areas [1]. Therefore, it is urgent to provide effective CMs for damaged areas.

In 2006, scientist Yamanaka discovered that Oct 3/4, Sox 2, KLF4 and c-Myc (OSKM) four transcription factors can reprogram mouse fibroblasts to embryonic stem cells (Embryonic stem cells, ESCs)-like pluripotent state cells, which are named induced pluripotent stem cells (iPSCs) [2]. Human induced pluripotent stem cells (hiPSCs) provide an infinite source of once-inaccessible human cell types for stem cell research and therapy [3,4], helping to mimic human disease and

Peer review under responsibility of KeAi Communications Co., Ltd.
* Corresponding author.
** Corresponding author.
*** Corresponding author.
**** Corresponding author.
E-mail addresses: 36163773@qq.com (M. Zhao), zhushuoji@gmail.com (S. Zhu), liu.nanbo@163.com (N. Liu), tanganqier@163.com (P. Zhu).
[1] These authors contributed equally to this work.

https://doi.org/10.1016/j.bioactmat.2022.05.024
Received 19 March 2022; Received in revised form 19 May 2022; Accepted 19 May 2022

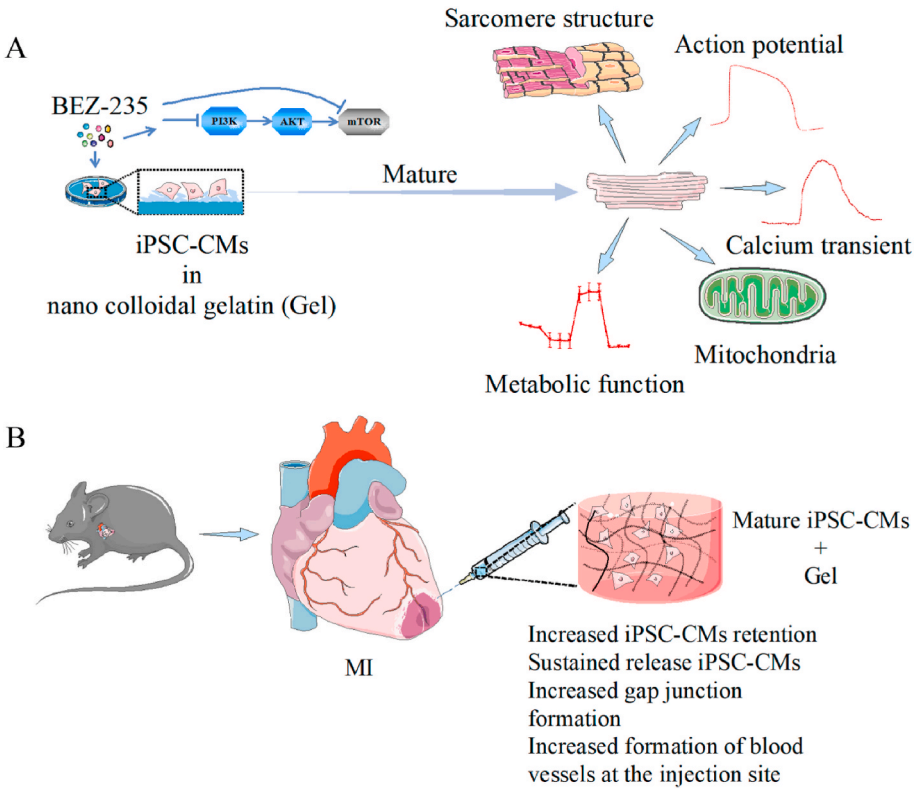

Scheme 1. (A) The mature strategy of iPSC-CMs. (B) Gel encapsulating mature iPSC-CMs for cardiac repair by injection into the MI area.

regenerate damaged tissues [5]. Importantly, scientists can also establish a research-grade human stem cell management system that is compatible with good laboratory practice, based on a tertiary biobank setup, for storage and distribution of high-quality and stable hiPSC cell lines [6]. With the deepening of research, iPSCs and different cell types derived from them have also entered the stage of clinical trials [7–10]. It can be seen that iPSCs are an important cell source for the establishment and treatment of many disease models. Subsequent studies have found that induced pluripotent stem cell-derived cardiomyocytes (iPSC-CMs) also have great potential in disease treatment because they avoid the socio-ethical issues of ESCs [11], while enabling provide an effective source of CMs for ischemic area. In the treatment of myocardial infarction (MI), iPSC-CMs can improve myocardial function, attenuates ventricular remodeling, and reduce mortality in infarcted rats [12]. However, there are still differences between iPSC-CMs and adult CMs, which are characterized by immaturity of cell structure and function, which will lead to fatal arrhythmias after transplantation [13], which is also the main bottleneck in the current treatment of iPSC-CMs.

Now, studies have successively revealed methods and strategies to promote the maturation of iPSC-CMs, including prolonging the culture time [14], triiodothyronine [15], dexamethasone (DEX) [16], fatty acids [17,18], electrical stimulation [19] and biomaterials [20], etc. Nonetheless, the underlying mechanisms have not been fully elucidated. We found that DEX was able to inhibit the expression of p-PI3K, *p*-AKT and *p*-mTOR in the above induction strategy [21], and the low expression of HIF-1α was associated with the inhibition of the PI3K/AKT/mTOR pathway [22]. HIF1α activation has also been shown to upregulate glycolytic enzymes, and glucose stimulation has been shown to inhibit the maturation of CMs [23]. Peroxisome proliferator-activator receptor alpha (PPARα) is highly expressed in cardiomyocytes and is a major transcriptional regulator of enzymes related to fatty acid metabolism. A study pointed out the inverse relationship between fatty acid metabolism/PPARα signaling and PI3K/AKT/insulin signaling observed in fatty acid-rich cultures is consistent with the metabolic switch detected in these cultures and is in agreement with the pattern reported for 1-year matured hESC-CMs [24,25]. Not only that, it has been confirmed that the inhibition of mTOR can make iPSC-CMs enter a quiescent state and improve the maturation of cellular sarcomeric structure, electrophysiology and metabolic function [26]. Taken together, we speculate that the PI3K/AKT/mTOR pathway may play an important regulatory role in the maturation of iPSC-CMs. On the other hand, the extracellular matrix (ECM) is an important supporting structure that provides dynamic signals in part through its chemical, physical and mechanical properties, and its main components include glycosaminoglycans, proteoglycans, protein fibers, glycoproteins and polysaccharides [27]. In the heart, the composition and distribution of the ECM varies with cardiogenesis [28] and affects cell contraction [29] and mitochondrial function [30]. Maturation of PSC-CMs can be achieved by adding ECM proteins and modulating substrate stiffness [31]. ECM component-derived hydrogels have also been extensively studied as cardiac tissue substitutes. Intercellular network formation, α-actinin and Cx43 expression, and contraction velocity were found to be increased in low-stiffness/fast-degrading and moderate-stiffness/moderate-degrading hydrogels, and an organized sarcomere structure was revealed and significantly increased contractile force [32]. Similarly, another study showed that neonatal rat cardiomyocytes (NRCM) had better contractility in soft-matrix nanomaterials [33]. Interestingly, a softer ECM produced larger and more organized gap junctions than a hard surface, which was able to better promote the maturation of iPSC-CMs [34]. More importantly, soft-matrix biomaterials have also been shown to provide a good medium for the treatment of MI [35]. It can be seen that the growth and maturation of cells in vitro requires certain structural support.

In summary, we speculate that by inhibiting the PI3K/AKT/mTOR pathway and providing additional structural support to cells, the maturation of iPSC-CMs can be more favorable. In this study, we synthesized a collagen-based nano colloidal gelatin (Gel) as a medium for cell growth in vitro according to the composition of ECM. At the same time, the combined effect of PI3K/AKT/mTOR pathway inhibitor BEZ-

235 on the maturation of iPSC-CMs has been confirmed in this study (Scheme 1A). Finally, we encapsulated mature iPSC-CMs with gelatin, resulting in increased gap junction formation in the MI region and enhanced angiogenesis (Scheme 1B). In conclusion, BEZ-235 combined with Gel can promote the maturation of iPSC-CMs, and the encapsulation of mature iPSC system with Gel can bring benefits to the treatment of myocardial infarction.

2. Experimental section

2.1. Materials and reagents

Gelatin was purchased from Rousselot Co., Ltd (Guangzhou, China). Human induced pluripotent stem cells (hiPSCs) was purchased from Renovation Biotech Co., Ltd (Hangzhou, China). C57BL/6 was purchased from Guangdong Medical Laboratory Animal Center (Guangzhou, China).

2.2. Synthesis of gel

Gelatin solution was obtained by dissolving gelatin in distilled water under heating at constant temperature. Acetone (Aladdin, China) was added to the gelatin solution to precipitate high molecular weight gelatin. After redissolving the precipitate in 10 ml water at 50 °C, cooling to room temperature and adjusting the pH of the gelatin solution to 2.5, acetone was added dropwise to the vigorously stirred gelatin solution to form gelatin nanospheres. Subsequently, the nanoparticles were cross-linked with glutaraldehyde (Aladdin, China) overnight. After 16 h of cross-linking, the glycine solution was added to the nanosphere suspension, and the suspension was subjected to three cycles of centrifugation (13200 rpm, 5min) and resuspended in deionized water by vortexing, followed by pH adjustment to 7.0. After lyophilization, nanocolloidal gelatin (Gel) was stored at 4 °C until further use.

2.3. Fourier transform infrared spectroscopy (FTIR) test

FTIR (Thermofisher, USA) was used to monitor double network colloidal gel complexation behavior. During the test preparation, Gel was lyophilized and put into a quartz mortar for repeated grinding to obtain gel powder. FTIR spectra were measured in transmission mode with a spectral resolution of 4 cm^{-1} and a scan speed of 0.2 cm/s, 10 scans per measurement, and their representative spectra were used for further analysis.

2.4. Detection of gel-forming ability

We weighed Gel powders of different masses and dissolved them in PBS buffer to make solutions of 3%, 4%, 5%, and 6% concentration respectively. The above solutions were quickly pipetted evenly, adjusted to pH7.0 and transferred into the gel-forming vial. Let stand at room temperature, during which the gel-forming vial is turned upside down every 15min to observe the gel-forming situation and time.

2.5. Rheological test

Detection was performed using an AR2000ex rheometer (TA Instruments, USA) with flat steel plate geometry (40 mm diameter). The test temperature was set at 25 °C and the operating gap was 1000 μm. Time sweeps were all performed at a shear frequency of 1 Hz and a strain of 0.5%. The frequency sweep of the samples was set from 0.1 to 100 Hz with a constant shear strain of 0.5%.

2.5.1. Electron microscopy

For scanning electron microscopy (SEM; Hitachi S–3400 N, Japan), the material was placed on the SEM stage, coated with gold by vacuum spraying for 90s, and the acceleration voltage was 10kv for observation.

For transmission electron microscopy (TEM; Hitachi H800, Japan), the material was diluted and dispersed with ultrapure water at 0.05% mass fraction, and then dripped onto a copper grid for sample preparation. Blot the excess liquid on the edge with filter paper, place the copper mesh in a drying container overnight, observe and photograph by TEM.

2.6. Gel degradation test in vitro

PBS containing collagenase type I (Sigma, USA) and sodium azide (Merck, USA) was prepared and incubated with 5% Gel in a 37 °C oven. At different time points, 2767 g, centrifuged for 5min, 0.9 ml of supernatant was collected after separation of gelatin particles for protein quantitative determination with BCA Protein Assay Kit (KeyGen, China), the degradation rate-time curve was drawn, and the same volume of fresh collagenase solution was added at the same time.

2.7. Extraction of NRCM

1–3 days old SD rats were sterilized in 75% alcohol, the left rib of the sternum was cut vertically, the heart was extruded from the thoracic cavity, the left ventricle was clipped, rinsed twice, and torn into strips, and digested in trypsin (Gibco, USA) for 10 h at 4 °C. The tissue blocks were soaked in DMEM medium (Gibco, USA) containing 10% FBS (Gibco, USA), and the digestion was terminated in a 36 °C water bath for 5min. Collagenase type I was added, and the mixture was digested at a constant temperature of 100 rpm with magnetic stirring for 15min. Let stand for 5min, take the supernatant, add DMEM medium containing 10% FBS to terminate the digestion, centrifuge at 800 rpm for 3min, discard the supernatant, add an appropriate amount of DMEM medium containing 10% FBS, and inoculate a new cell suspension after pipetting evenly in a culture dish, the cells were cultured at 37 °C in a 5% CO_2 incubator for 2 h at differential speed. Subsequently, the supernatant was transferred to a new culture dish and cultured for 2 h, and the cell supernatant at this time was transferred to a 15 ml centrifuge tube for later use.

2.8. Gel cytotoxicity assay in vitro

We prepared 4%, 5%, and 6% Gel, without Gel as control, spread them evenly into 24-well plates, left standing at room temperature for 30min, inoculated the prepared NRCM on the surface of Gel, shaken it horizontally, and placed it at 37 °C, 5% CO_2 cultured in an incubator. According to the instructions of the Live/Dead staining kit (Dojindo, Japan), the extensibility and viability of the cells were detected on the 1st and 7th day, respectively, and the live and dead cells were observed under the fluorescence microscope (Leica, Germany).

2.9. Gel toxicity assay in vivo

The MI mouse were injected intramyocardially with PBS and Gel, two injection sites were set in each heart, each injection site was 10 μl, and the ear tags were marked. After 7 days, 200 μl of mouse apical arterial blood was drawn, and the serum levels of Alanine transaminase (ALT) and Aspartate aminotransferase (AST) were used as indicators of liver function while serum levels of Blood Urea Nitrogen (BUN) and Creatinine (Cr) were used as indicators of renal function. Serum concentrations of ALT, AST, BUN and Cr were analyzed by enzyme-linked

immunosorbent assay (ELISA; Moshake Biotechnology, China) in accordance with the manufacturer's instruction. At the same time, CD68 (Abcam, 1:300) immunofluorescence staining was performed on mouse hearts to evaluate macrophage infiltration.

2.10. iPSCs culture and CMs differentiation

iPSCs were seeded in Matrigel-coated (Corning, USA) dishes diluted 1:100 with DMEM/F12 (Gibco, USA), and cultured with mTeSR™ Plus complete medium (Stem Cell, USA) at 37 °C in a 5% CO_2 incubator. iPSCs were passaged with Accutase™ (Stem Cell, USA) once confluence reached 85% confluence using and cultured in mTeSR™ Plus complete medium supplemented with 5 μM Y-27632 (Selleck, USA) for 18 h prior to maintenance in mTeSR™ Plus complete medium.

CMs differentiation was performed with reference to previous studies [36]. Briefly, cells were cultured and expanded to 90% cell confluence, and then treated for 2 days with 6 μM CHIR-99021 (Selleck, USA) in RPMI-1640 (Gibco, USA) and B27 supplement minus insulin (RPMI-1640 + B27-insulin) (Gibco, USA) to activate the Wnt signaling pathway. On day 2, cells were placed in RPMI-1640 + B27-insulin with CHIR-99021 removal. On days 3–4, cells were treated with 5 μM IWR-1 (Selleck, USA) to inhibit the Wnt signaling pathway. On days 5–6, cells were removed from IWR-1 treatment and placed in RPMI-1640 + B27-insulin. From day 7 onwards, cells were placed and cultured in RPMI-1640 and B27 supplement with insulin (RPMI-1640 + B27) (Gibco, USA) until beating was observed.

2.11. Flow cytometry

Cardiomyocytes were obtained with trypsin and fixed in 4% PFA for 20 min. Cells were permeabilized with 0.1% Triton-X 100 for 10 min. The following primary antibodies were applied: rat *anti*-cTnT (BD, USA). The stained cells were counted using BD FACS Calibur. The following data analysis was performed using FlowJo software.

2.12. Quantitative real time PCR

Total RNA of iPSCs or iPSC-CMs extraction using RNA simple Total RNA kit (Tiangen, China) in accordance with the manufacturer's instruction. cDNA was synthesized with Bestar™ qPCR RT Kit (DBI, Germany). And quantative real time PCR (qRT-qPCR) was conducted using Bestar^R SybrGreen qPCR kit (DBI, Germany) with the following method: 2min at 95 °C, followed by 40 cycles (95 °C for 10s, 60 °C for 34s and 72 °C for 30s), 95 °C for 1min, 55 °C for 1min. The primer sequences were listed in Table S1. GAPDH was used as the housekeeping gene. Relative gene expression of target genes was quantified relative to GAPDH, a housekeeping gene, and calculated using the $2^{-\Delta\Delta Ct}$.

2.13. Western blot

Western blot was performed with reference to previous studies [37]. Protein of iPSC-CMs were extracted using RIPA protein extraction solution (Beyotime, China) supplemented with protease inhibitor (Beyotime, China) and phosphatase inhibitor (Beyotime, China) on the ice for 30min. The extracted proteins were determined by BCA Protein Assay Kit (KeyGen, China). The proteins were separated using SDS-PAGE and transferred to PVDF membranes (Millipore, MA). After blocking with 5% milk for 2 h at room temperature, the membranes were incubated antibodies against rabbit *anti-p*-AKT, t-AKT, *p*-mTOR, t-mTOR, p-70s6k, t-70s6k, p-4EBP1 and t-4EBP1 (Abcam, 1:1000) overnight at 4 °C. After being rinsed for three times with Tris buffered solution (TBST) (Solarbio, China), the membrane was incubated in goat anti rabbit secondary antibodies conjugated with horseradish peroxidase (HRP) (Bioss, 1:5000) for 2 h at room temperature. And labeled proteins were visualized using the ECL chemiluminescence reagent (Biorad, USA). Densitometric analysis was determined using ImageJ analysis software and β-Tubulin was used as an internal standard.

2.14. Cell number counting and cell counting Kit-8 (CCK-8) test

In order to evaluate the effect of different concentrations of BEZ-235 (Selleck, USA) on the viability of iPSC-CMs, we detected the change of cell number before and after drug addition and reflected the cell viability by cell counting and CCK-8 assay. Specifically, the initial cell number was recorded by a cell counter before iPSC-CMs were seeded. After the iPSC-CMs were treated with different concentrations of BEZ-235 for 7 days, the cells were digested and resuspended, and the cells were counted again.

The detection was performed according to the instructions of the CCK-8 kit (Dojindo, Japan). Specifically, iPSC-CMs cells were digested, resuspended and seeded in a Matrigel-coated 96-well plate, added with RPMI-1640 + B27 medium containing 10% CCK-8, and placed at 37 °C, 5% CO_2 incubator and incubated for 1 h. The absorbance at 450 nm was measured by Varioskan LUX Multimode Microplate Reader (Thermofisher, USA). Collect data for analysis.

2.15. Maturation process of iPSC-CMs

We prepared 4%, 5%, and 6% Gel, spread them evenly into 6-well plates, left standing at room temperature for 30min, then added matrigel on the surface of the Gel and incubated it in a 37 °C, 5% CO_2 incubator for 1 h. iPSC-CMs were digested and plated on the surface of plates with or without Gel. RPMI-1640 + B27 medium with or without BEZ-235 was added for 5 days after iPSC-CMs were plated.

2.16. Immunofluorescence

Immunofluorescence of cells was performed in confocal dishes, and cells were fixed with 4% paraformaldehyde (Beyotime, China) for 30 min at room temperature. Samples were permeabilized with 0.3% Triton X-100 (Solarbio, China) for 20min at room temperature and blocked with goat serum (Beyotime, China) for 1 h at room temperature. For iPSCs, mouse SSEA4 primary antibody (Abcam, 1:300) and rabbit OCT4 primary antibody (Abcam, 1:200) were added simultaneously. For iPSC-CMs, mouse cTnT primary antibody (Thermofisher, 1:40) and rabbit α-Actinin primary antibody (Abcam, 1:500) were added simultaneously. The above primary antibodies were incubated overnight at 4 °C. For iPSCs, goat anti-mouse 555 and goat anti-rabbit 488 secondary antibodies (Bioss, 1:1000) were added simultaneously. For iPSC-CMs, goat anti-mouse 488 and goat anti-rabbit 555 secondary antibodies (Bioss, 1:500) were added simultaneously. The above secondary antibodies were incubated for 1 h at room temperature in the dark. Nuclei were counterstained with DAPI staining solution (Beyotime, China) and incubated at room temperature for 10 min. Images were captured by a laser scanning confocal microscope (Leica, Germany) and analyzed with Leica Application Suite X software.

2.17. Patch clamp for action potential recordings

Extracellular fluid: 150 mM NaCl, 5.4 mM KCl, 1 mM $MgCl_2$, 10 mM glucose, 1.8 mM $CaCl_2$ and 10 mM HEPES, adjusted to pH = 7.4 with NaOH. Electrode internal solution: 150 mM KCl, 5 mM NaCl, 2 mM $CaCl_2$, 10 mM HEPES, 5 mM Mg-ATP and 5 mM EGTA, adjusted to pH = 7.2 with KOH. The glass electrode was put into MODEL P97 for electrode stretching, and the temperature was kept at 35.5–37 °C. The extracellular perfusate is used for perfusion, and the drawn electrode is pressed down into the liquid and lightly pressed on the cells, followed by sealing and rupture of the membrane. Recording was performed using an EPC-10 amplifier and a PatchMaster (HEKA, Germany) for data acquisition with a sampling frequency of 10 kHz.

2.18. Calcium transient

The perfusate was prepared: 150 mM NaCl, 5.4 mM KCl, 1 mM $MgCl_2$, 10 mM glucose, 1.8 mM $CaCl_2$ and 10 mM HEPES, adjusted to pH = 7.4 with NaOH. iPSC-CMs were digested into single cells, seeded on Matrigel-coated coverslips at appropriate density, incubated with 5 μM Fluo-4/AM (Dojindo, Japan) at room temperature for 15min, and then continuously perfused with perfusate. Calcium transients were recorded by a CCD on an inverted fluorescence microscope (Nikon, Japan) and data were acquired by NIS-Elements software. Calcium transient amplitudes are measured as relative values (ΔF/F0). Statistics and analysis of the data were performed using Igor Pro (Wavemetrics, USA).

2.19. Cell microelectrode arrays (MEA) detection

The iPSC-CMs were digested into single cells and seeded in Matrigel-coated 6-well MEA electrodes with a cell number of 1×10^5/well. The MEA electrode plate was carefully moved into the incubator for 30min, and 500 μl of medium was added after waiting for the cells to adhere. After the cells resumed regular beating, the MEA2100 acquisition system (Multi Channel Systems, Germany) was used to record the spontaneous beating field potential of iPSC-CMs with a sampling frequency of 10 kHz. Data were analyzed with Cardio $2D^+$ software (Multi Channel Systems, Germany).

2.20. Mitochondrial membrane potential test

The mitochondrial membrane potential was detected according to the instructions of the mitochondrial membrane potential kit (JC-1, Beyotime, China). Briefly, iPSC-CMs were digested into single cells and seeded in Matrigel-coated 12-well plates. 48 h after cells adhered, 1 × JC-1 staining working solution was added and stirred well. Incubate for 20min in a 37 °C, 5% CO2 incubator. After the incubation, the JC-1 staining working solution was removed and washed twice with 1 × JC-1 staining buffer. Observed and photographed under a fluorescence microscope.

2.21. TEM detection of cellular mitochondrial microstructure

For cell TEM, firstly add glutaraldehyde to the culture plate, gently scrape the cells with a cell scraper to collect the cells into a centrifuge tube, centrifuge at 1000 rpm for 5min, discard the supernatant, add glutaraldehyde and gently pipet, and fix at room temperature for 2 h. After washing 3 times, it was fixed with 1% osmic acid, dehydrated with alcohol gradient (50%-70%-95%) after washing, infiltrated, embedded, and polymerized at 60 °C for 2 h. 60 nm ultrathin sections were made using an ultramicrotome and placed in copper grids in lead citrate staining solution.

2.22. Mitochondrial bioenergetic test

According to the manufacturer's instruction of the XF Cell Mitochondrial Stress Test kit (Agilent, USA), we detected the Oxygen consumption rate (OCR) of iPSC-CMs. Specifically, iPSC-CMs were digested into single cells, and after cell counting, 3.2×10^4 cells were seeded in each well of an XFe 96 cell culture plate, and cultured in a 37 °C, 5% CO_2 incubator for 24 h. Preheat the machine and hydrate the sensor cartridge ahead of time. In 97 ml of Seahorse XF RPMI medium, 1 ml of glucose, 1 ml of pyruvate and 1 ml of L-glutamine were added and mixed to form the detection solution. The detection solution was added to the cell plate, and it was placed in a 37 °C, CO_2-free incubator for 1 h. Oligomycin (1.5 μM), carbonyl cyanide p-(trifluoromethoxy) phenylhydrazone (FCCP) (1 μM) and rotenone (Rot, 0.5 μM)+antimycin A (AA, 0.5 μM) were added to sensor cartridge ports in sequence. Immediately insert the cell culture microplate into the XF96 Extracellular Flux Analyzer (Agilent technologies, USA) and run the Cell Mitochondrial Stress Test. After measuring OCR, cells were lysed and the protein in each well was quantified using the BCA protein quantification kit. All values of OCR parameters calculated were normalized to the quantified protein content. Data were analyzed using Wave software (Agilent technologies, USA).

2.23. Establishment of MI model and evaluation of treatment effect of iPSC-CMs

Male C57BL/6 mouse aged 6–8 weeks were anesthetized by intraperitoneal injection with 1% sodium pentobarbital at a dose of 50 mg/kg. Positive pressure ventilation was performed after tracheal intubation, the respiratory rate was 110 times/min, the respiratory ratio was 5:4, and the tidal volume was about 3 ml. The left anterior descending coronary artery was ligated with 8–0 prolene atraumatic suture at 1 mm from the lower edge of the left atrial appendage, with a depth of about 0.5 mm and a width of about 1 mm. After successful ligation, the myocardial tissue at the anterior wall of the left ventricle and the apex of the heart were observed to be white, and the activity of the ventricular wall was significantly weakened, and the MI modeling was determined to be successful.

iPSC-CMs were labeled with 1 μM of CM Dil (Thermofisher, USA). According to the experiment, we divided into 4 groups: PBS group, immature iPSC-CMs group (Immature): iPSC-CMs not treated with BEZ-235 or Gel, mature iPSC-CMs group (Mature): iPSC-CMs treated with BEZ-235 + Gel, Gel + mature iPSC-CMs group (Gel + mature): the iPSC-CMs treated with BEZ-235 + Gel were digested and mixed with 5% Gel. Among them, for the Gel + mature group, 5% Gel needs to be prepared, and the cell suspension and Gel are mixed evenly so that the cell density is 1×10^7/ml. Immature and Mature simply resuspend the cells at a density of 1×10^7/ml. After the MI model was successfully established, 20 μl of each system was immediately transplanted in situ and injected into 2 points in total.

Immunofluorescence of frozen sections of cardiac tissue, fixed with 4% paraformaldehyde for 30min. EDTA antigen retrieval buffer for antigen retrieval. BSA was added dropwise and blocked at room temperature for 30min. Incubation primary antibodies: rabbit CD68 primary antibody (Servicebio, 1:300), rabbit Ki67 primary antibody (Servicebio, 1:1000), rabbit Cx43 primary antibody (Servicebio, 1:300), rabbit CD31 primary antibody (Servicebio, 1:300), rabbit α-SMA primary antibody (Abcam, 1:300), mouse cTnT primary antibody (Servicebio, 1:500), both were incubated overnight at 4 °C. Incubate with secondary antibodies: Alexa Fluor 488-labeled goat anti-rabbit IgG (Servicebio, 1:500), Cy5-labeled goat anti-mouse IgG (Servicebio, 1:500), and incubated for 1 h at room temperature in the dark. DAPI was added dropwise and incubated at room temperature in the dark for 10min to counterstain the nuclei. Images were captured by a laser scanning confocal microscope (Leica, Germany) and analyzed with Leica Application Suite X software.

2.24. Statistic analysis

All data were statistically analyzed and plotted using the software SPSS 20 and Graphpad prism 8.0. The data between multiple groups were analyzed by one-way analysis of variance (ANOVA). When the data between the two groups met the normal distribution, the independent sample *t*-test was used, and when the data did not meet the normal distribution, the nonparametric test was used. $P < 0.05$ was considered statistically significant. All experiments were performed at least three times. Among them, for the measurement of sarcomere structure of cardiomyocytes, at least 32–53 cells in each group were selected for analysis; for the measurement of action potentials, at least 22–35 cells were selected in each group, and for the measurement of calcium transients, at least 20–29 cells were selected in each group. For animal experiments, 3 animals were selected from each group. All measurement data were expressed as mean ± standard deviation (mean ± SD).

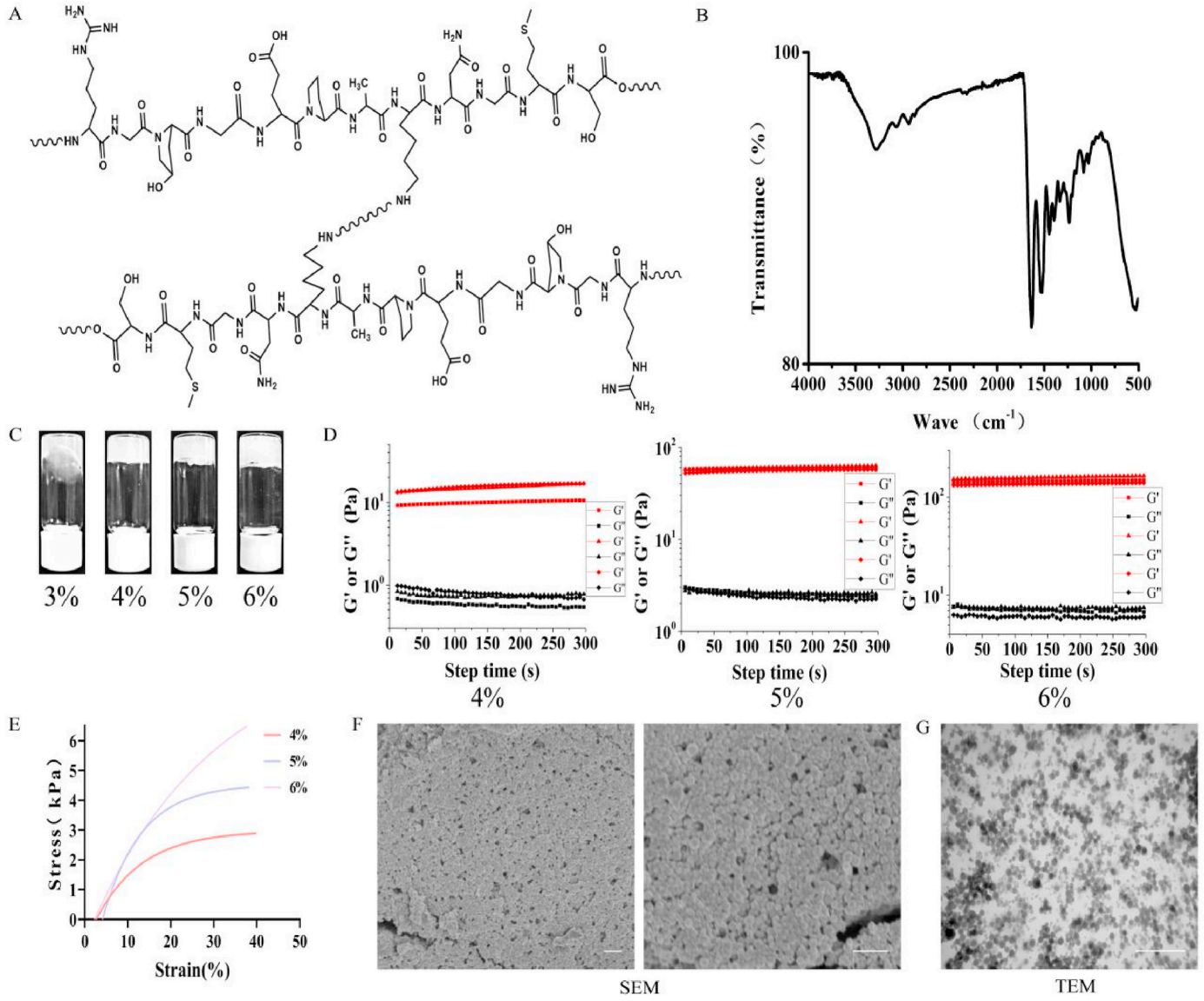

Fig. 1. Characterization of Nanocolloidal Gelatin. (A) Gel molecular structure. (B) Gel composition analysis. (C) Gel-forming property testing of different concentrations of Gel. (D) Rheological detection of different concentrations of Gel. (E) Stiffness of Gel at different concentrations. (F) Representative SEM image of Gel. (G) Representative TEM image of Gel. Scale bar = 500 nm.

3. Results and discussion

3.1. Preparation and performance testing of gel

Collagen, the most widely distributed ECM protein in the body, is important for maintaining the function of organs and tissues, and also plays an important role in determining the overall mechanical and metabolic properties of tissues [38]. Here, we prepared Gel by a two-step method, and its chemical composition was detected by FTIR. The main characteristic peak distribution of the material is: The characteristic peak of the amide I band (stretching vibration of the C═O bond in the amide group) is located at the wavelength of 1632 cm^{-1}. The amide II band (the sum of N–H bending vibrations and C–N stretching vibrations in the amide group) is located at 1539 cm^{-1}, the amide III band (the synchronous addition of N–H bending vibrations and C–N stretching vibrations) is located at 1447 cm^{-1}, amide A band (the sum of the stretching vibration of the N–H group in the amide bond and the stretching vibration of the O–H group) forms a broad peak at the wavelength of 3286 cm^{-1}, and the stretching vibration peak of –COO– is located at 1300-1450 cm^{-1} (Fig. 1A and B) (Table S2). The above data proves that the chemical composition of the material is the chemical composition of typical collagen-based materials, with typical characteristic peaks of amide groups, and characteristic peaks of other chemical substances are not observed.

In order to test the gel-forming ability of Gel, we prepared gelatin with 3%, 4%, 5%, and 6% concentration respectively, adjusted the pH value to 7.0, and transferred it into a gel-forming vial. Among them, 4%–6% concentration of Gel can be able to form stable colloid, which appears as a white jelly. However, Gel with a concentration of 3% still could not form a stable colloid after prolonging the gelation time, and the fluidity was large (Fig. 1C). Therefore, we chose 4%–6% concentration of Gel as follow-up experiments. We explored the mechanical properties of 4%, 5%, and 6% Gel. As shown in Fig. 1D, the elastic modulus (G′) of different concentrations of Gel was greater than the viscous modulus (G″), indicating that 4%, 5% and 6% concentration of Gel can form a stable colloid. Among them, the G′ value of 4% Gel was 10.01 ± 0.41 Pa, the G′ value of 5% Gel was 59.44 ± 0.86 Pa, and the G′ value of 6% Gel was 146.50 ± 2.49 Pa. The mechanical property of the different concentrations of Gel were evaluated (Fig. 1E). The stress appeared an increasing tend along with the strain increasing in every

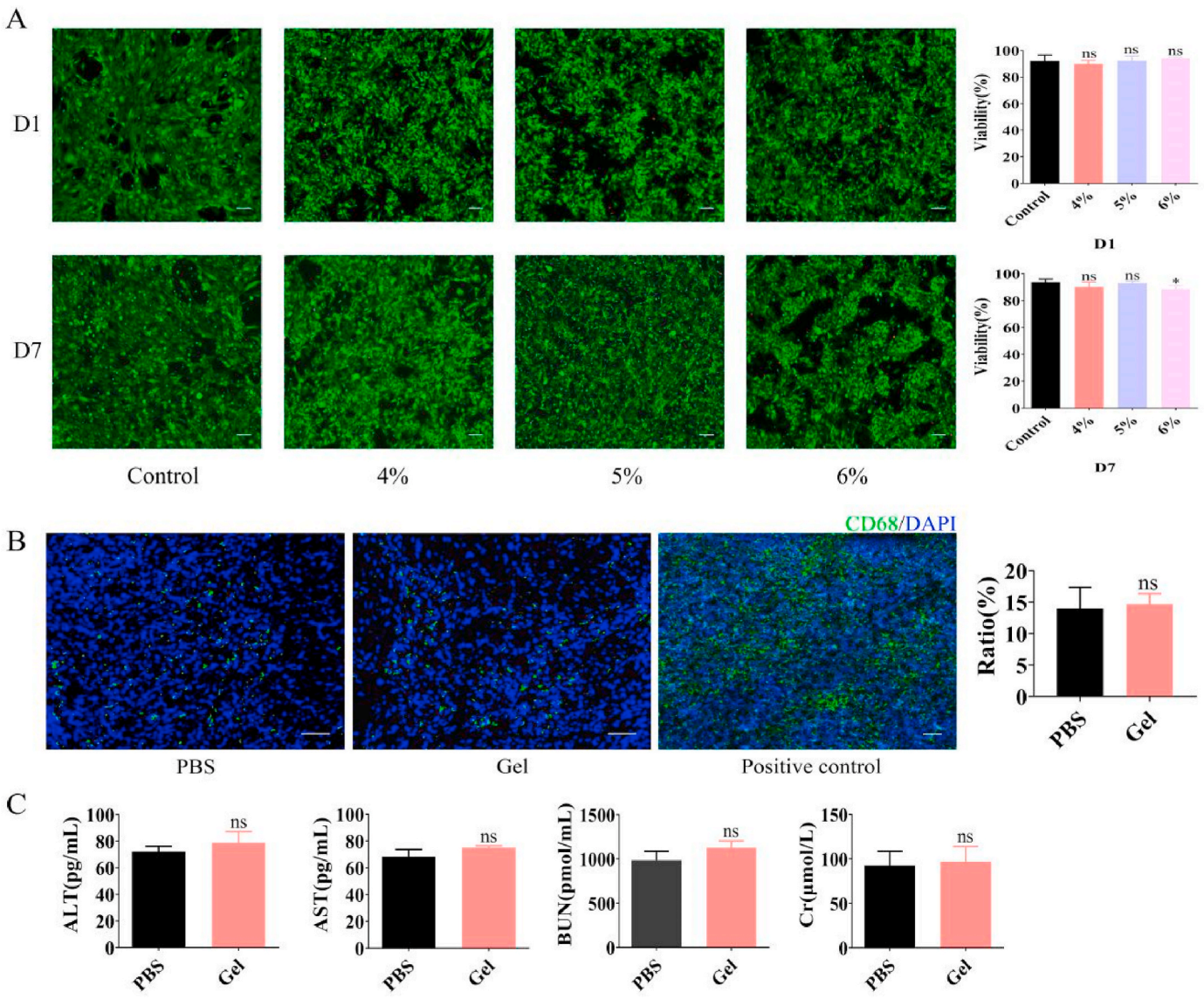

Fig. 2. Biocompatibility Analysis of Gel. (A) Cell viability of NRCM grown on the surface of Gel with different concentrations at 1 and 7 days. *P < 0.05 vs. control. ^{ns}P>0.05 vs. Control. n = 3. Scale bar = 100 μm. (B) Representative CD68 immunofluorescence of macrophages. n = 3. Scale bar = 50 μm. (C) Evaluation of liver and kidney function in mouse. ^{ns}P>0.05 vs. Control. n = 3.

sample before it reached yield strain. We observed the morphology of Gel by electron microscopy and found that micro-nano particles of different sizes were present (Fig. 1F and G).

3.2. Degradation and biocompatibility testing of gel

To determine the cytocompatibility of Gel at 4%, 5%, and 6% concentrations, we seeded NRCM on the surface of Gel and assessed cell viability on Gel by Live/Dead staining. On the first day after inoculation of NRCM, there was no significant difference in cell viability between different concentrations. Over time, when NRCM was grown on the surface of 6% Gel to day 7, the cell viability was reduced compared to the control group, while the viability of cells grown on 4% and 5% Gel was not significantly affected (Fig. 2A). A similar effect was also observed in iPSC-CMs (Fig. S1). Previous studies have shown that soft-matrix biomaterials are more able to promote the maturation of iPSC-CMs [34], and the corresponding G′ at 5% concentration is also similar to that of collagen gels reported in a recent study, confirming that it is suitable for growth of iPSC-CMs [39], so we chose 5% concentration of Gel for subsequent studies.

We used BCA experiment to detect the degradation rate of Gel in different concentrations (0, 70U/ml, 140U/ml, 280U/ml, 560U/ml) of collagenase type I solution. The degradation rate in 11-day PBS solution without collagenase type I was only (5.93 ± 0.57)%, and in PBS solution containing 70U/ml collagenase type I in 11-day degradation rate (35.52 ± 0.66) %, the 11-day degradation rate in 140U/ml collagenase type I in PBS solution was (38.34 ± 2.93)%, and the 11-day degradation rate in 280U/ml collagenase type I in PBS solution (57.90 ± 2.93)% 6.19)%, while it was almost completely degraded in 560U/ml collagenase type I in PBS for 9 days (Fig. S2).

As a carrier of cells, biomaterials should not have tissue inflammation and liver and kidney toxicity [40]. We have successfully established a mouse model of myocardial infarction by ligating the anterior descending artery (Fig. S3). To evaluate the in vivo biosafety of Gel, we injected it into the marginal zone of myocardial infarction in mouse after the establishment of the MI model, and performed CD68 immunofluorescence staining on day 7 post-injection. As shown in Fig. 2B, the results showed that there was no statistical difference in the proportion of macrophages between the different groups. Next, we detected the liver and kidney function of the mouse in each group, and there was no

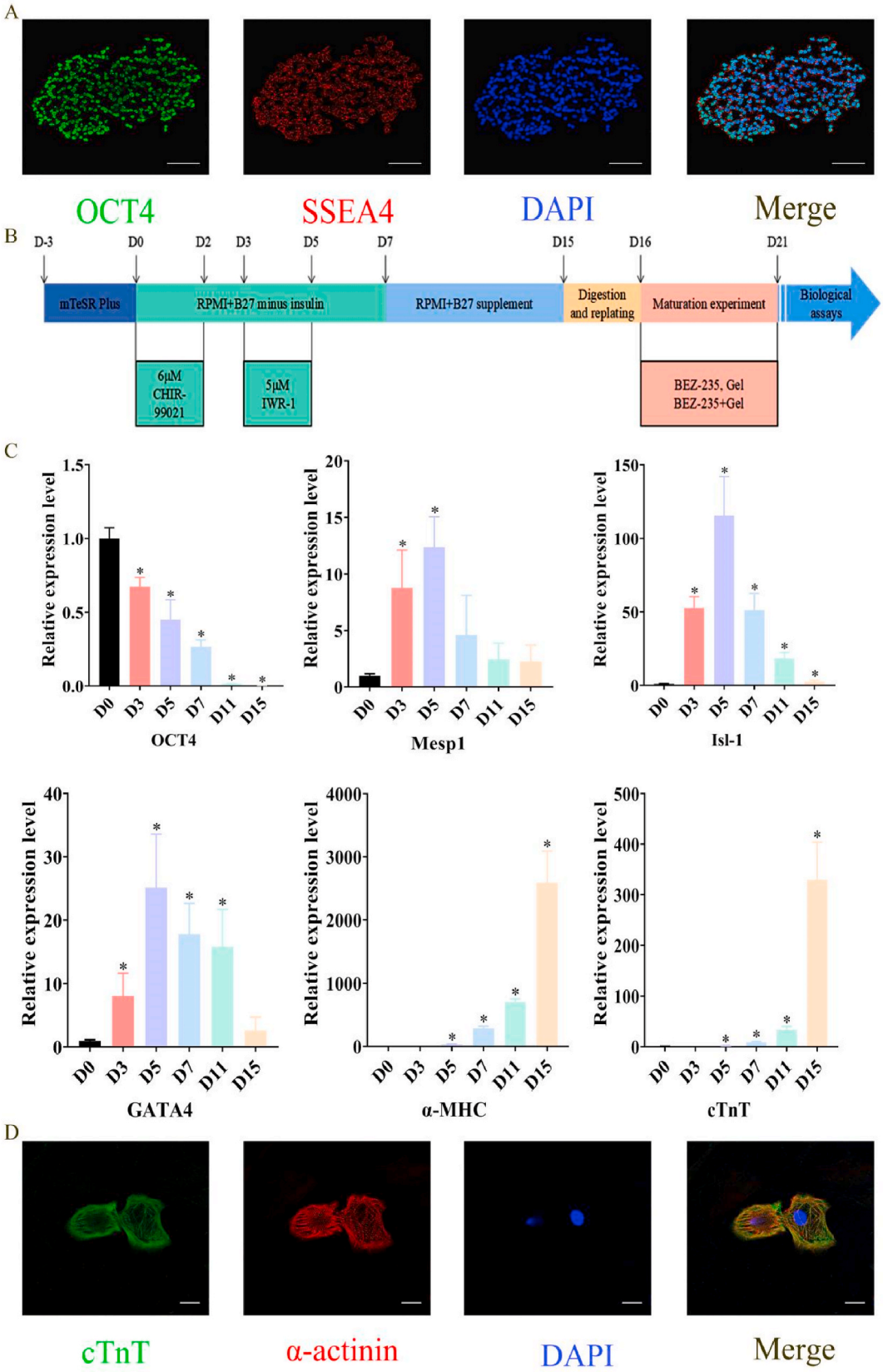

Fig. 3. Characteristics of iPSCs and iPSC-derived CMs. (A) Immunofluorescence images indicate that iPSCs express pluripotent stem cell-specific markers octamer-binding transcription factor (OCT4, green), stage-specific embryonic antigen-4 (SSEA4, red), and nucleus (blue). n = 3. Scale bar = 100 μm. (B) Schematic depicting the process of iPSCs culture, differentiation, and maturation of iPSC-CMs. (C) Expression of Oct4, Mesp1, Isl-1, Gata4, α-MHC and cTnT in the spontaneously differentiated iPSC-CMs. *P < 0.05 is indicated as results of indicated day vs. day 0 (D0). n = 3. (D) iPSC-CMs expressed cardiomyocyte-specific markers cardiac troponin T (cTnT, green) and sarcomeric α-actinin (red). n = 3. Scale bar = 20 μm.

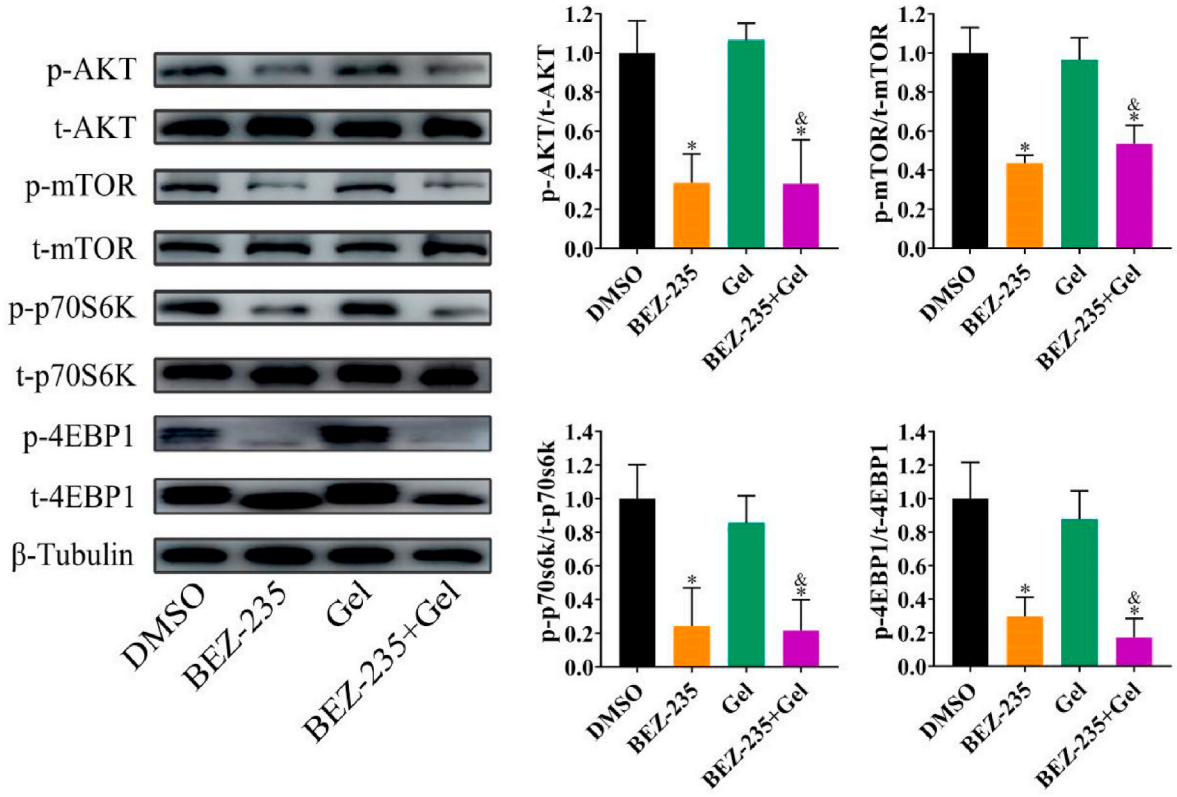

Fig. 4. Effects of BEZ-235 + Gel on PI3K/AKT/mTOR pathway. *P < 0.05 vs. DMSO, &P < 0.05 vs. Gel. n = 3.

statistical difference in serum ALT, AST, BUN and Cr concentrations among the groups. The above results show that the orthotopic injection of Gel into the mouse heart did not cause myocardial tissue inflammation and liver and kidney function damage. Taken together, we believe that Gel can support cell culture in vitro and serve as a delivery vehicle in vivo (Fig. 2C).

3.3. Culture of iPSCs and differentiation of CMs

It has been reported that the morphology of iPSCs colonies is a key factor affecting their pluripotency [41]. After 3 days of culture on Matrigel, we observed that the cells grew in colonies with rounded edges. The detection can be observed that the stem cell specific marker OCT4 is expressed in the nucleus and SSEA4 is expressed on the cell surface. This indicates that iPSCs are pluripotent (Fig. 3A).

Subsequently, we induced the generation of CMs using a classical method (Fig. 3B), and spontaneously beating CMs were observed on day 7. The differentiation efficiency of iPSC-CMs is about 83% (Fig. S4). Next, we examined gene expression levels of specific markers at different differentiation stages (Fig. 3C). Undifferentiated iPSCs (Day 0) highly expressed Oct4 stemness factor, and the expression gradually decreased with the passage of differentiation days. Mesoderm begins to express Mesp1 at day 3 and, similar to Isl-1, expression levels peaked at day 5 and decreased significantly at day 15, suggesting that cardiovascular lineage occurs during this period and that cardiac progenitors appear at day 7. As shown by Gata4, α-MHC, and cTnT assays, CMs began to beat spontaneously as early as day 7 and increased rapidly over the subsequent course. Differentiated cells were stained on day 12 to demonstrate the expression of α-actinin and cTnT CMs markers (Fig. 3D).

3.4. Inhibition of PI3K/AKT/mTOR by BEZ-235

In previous induction maturation protocols, we found that the PI3K/AKT/mTOR pathway may be involved in regulating the maturation of iPSC-CMs. Here, we selected BEZ-235, an inhibitor of the PI3K/AKT/mTOR pathway. To explore the inhibition of PI3K/AKT/mTOR pathway by different concentrations of BEZ-235 (0, 0.05, 0.1, 0.5, 1 μM), we detected the expression levels of *p*-AKT/t-AKT, *p*-mTOR/t-mTOR, p-p70S6K/t-p70S6K, p-4EBP1/t-4EBP1by WB. As shown in Fig. S5, the protein expression of *p*-AKT, *p*-mTOR, p-p70S6K, and p-4EBP1 gradually decreased with the increase of drug concentration starting from 0.05 μM of BEZ-235 concentration. However, when the concentration of BEZ-235 was 0.05 μM, the ratio of p-p70S6K/t-p70S6K, a downstream protein of the PI3K/AKT/mTOR pathway, was not significantly different from 0 μM (P > 0.05). At this concentration, BEZ-235 has not yet completely inhibited the PI3K/AKT/mTOR pathway.

We then examined the effect of different concentrations of BEZ-235 on cell viability. We seeded the same number of iPSC-CMs before administration, and 7 days later, we counted the cells under each drug concentration. We found that the number of iPSC-CMs treated with 0.5 and 1 μM concentrations significantly decreased compared with the 0 μM group (P < 0.05) (Fig. S6A). Based on this, we evaluated the cell viability, and the CCK-8 results corresponded to the cell count results, and the cell viability was significantly decreased at 0.5 and 1 μM concentrations (P < 0.05) (Fig. S6B). Based on the above results, we chose 0.1 μM concentration as the concentration for subsequent experiments.

In order to determine the optimal time of 0.1 μM BEZ-235, we selected the *p*-AKT/t-AKT, *p*-mTOR/t-mTOR, p-p70S6K/t-p70S6K, p-4EBP1/t-4EBP1 protein for different days of drug intervention (0, 0.5, 1, 3, 5, 7 day) for testing. As can be seen from Fig. S7, the protein expressions of *p*-AKT, *p*-mTOR, p-p70S6K, and p-4EBP1 were decreased in

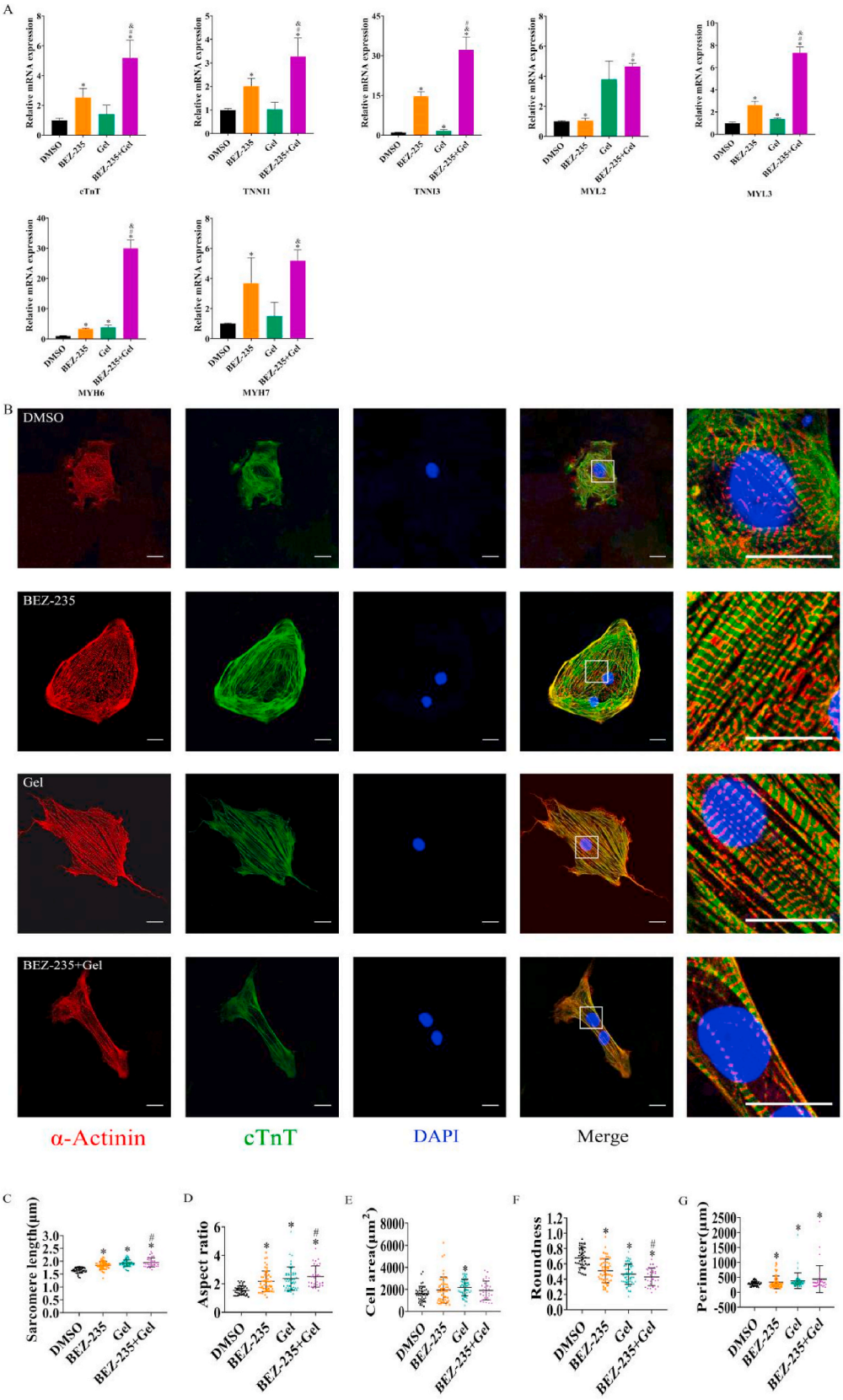

Fig. 5. BEZ-235 combined with Gel promoted morphological and structural changes of iPSC-CMs. (A) Expression of cardiac structural maturation markers detected by qRT-PCR. *P < 0.05 vs. DMSO, #P < 0.05 vs. BEZ-235, &P < 0.05 vs. Gel. n = 3. (B) Representative immunofluorescence images of sarcomeric α-actinin (red), cTnT (green) and DAPI (blue) in iPSC-CMs under different treatments. Scale bar = 20 μm. (C–G) Analysis of sarcomere length, aspect ratio, cell area, roundness and perimeter in iPSC-CMs. *P < 0.05 vs. DMSO, #P < 0.05 vs. BEZ-235, &P < 0.05 vs. Gel. n = 32–53 cells.

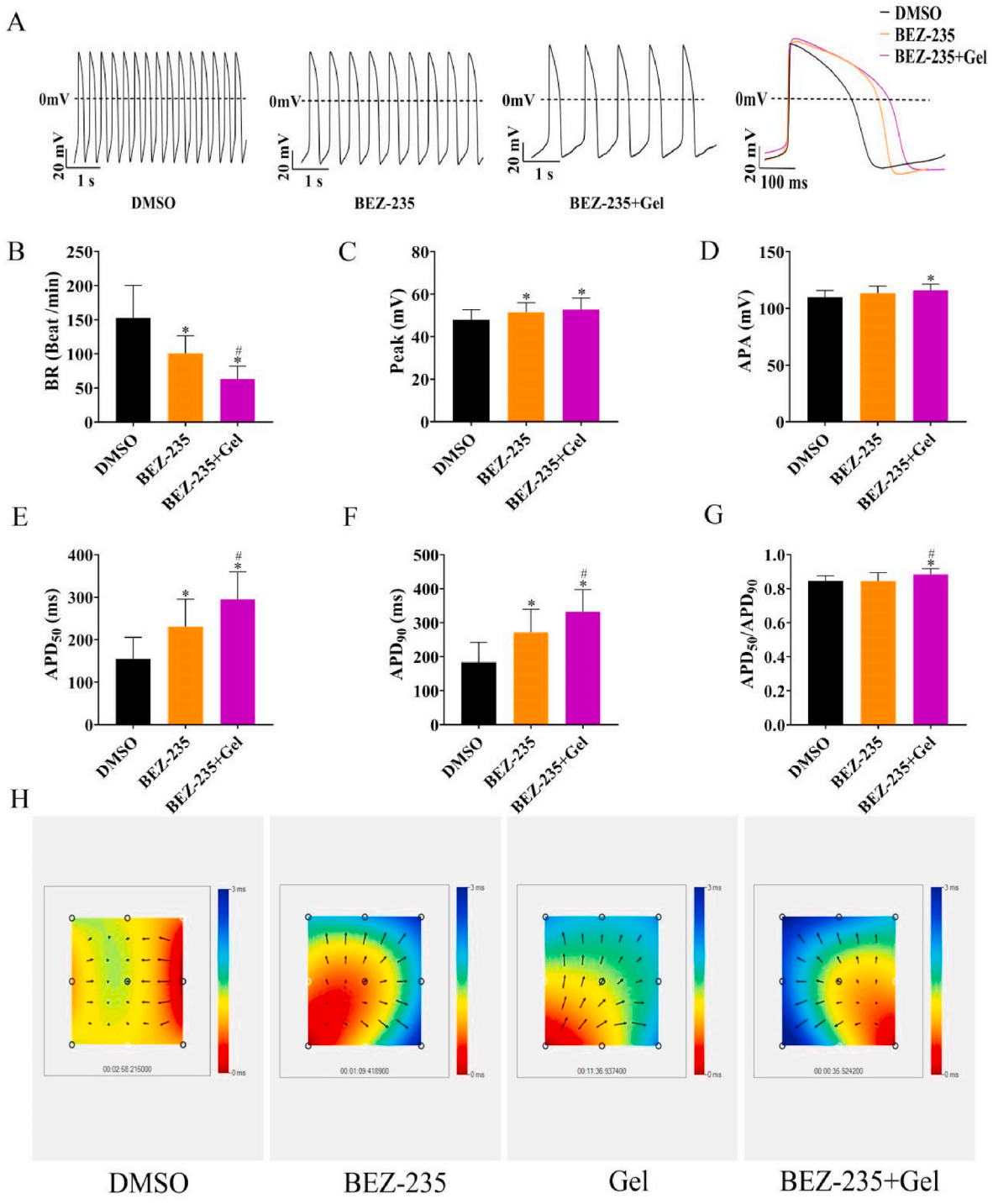

Fig. 6. BEZ-235 combined with Gel improved action potential maturation of iPSC-CMs. (A) Representative spontaneous action potential profile depicting. (B) Beat rate, (C) Peak, (D) APA, (E) APD50, (F) APD90 and (G) APD50/90. *P < 0.05 vs. DMSO, #P < 0.05 vs. BEZ-235, &P < 0.05 vs. Gel. n = 22–35 cells. (H) Representative color map of electrical signal propagation from each group of iPSC-CMs.

a clear time-dependent manner. For *p*-AKT/t-AKT, *p*-mTOR/t-mTOR decreased to the lowest level on the 5th day, while the expression of p-p70S6K/t-p70S6K,p-4EBP1/t-4EBP1 on the 5th day was almost the same as that on the 7th day, and there was no obvious decrease. Based on the above data, we chose BEZ-235 at a concentration of 0.1 μM in the follow-up experiments, and the effect time was 5 days.

We further tested whether synthetic Gel had an effect on the PI3K/AKT/mTOR pathway, and cultured iPSC-CMs in the environment containing DMSO (control), BEZ-235, Gel, and BEZ-235 + Gel, respectively. When iPSC-CMs were cultured in BEZ-235, BEZ-235 + Gel, the protein expressions of *p*-AKT, *p*-mTOR, p-p70S6K, p-4EBP1 decreased, while the phosphorylated proteins of DMSO group and Gel group showed no significant difference. Secondly, compared with the Gel group, the expression of phosphorylated proteins in the BEZ-235 + Gel group was down-regulated (P < 0.05), while there was no significant difference in the expression of phosphorylated proteins compared with the pure BEZ-235 group (P > 0.05) (Fig. 4). The above results indicated that Gel had no effect on the PI3K/AKT/mTOR pathway.

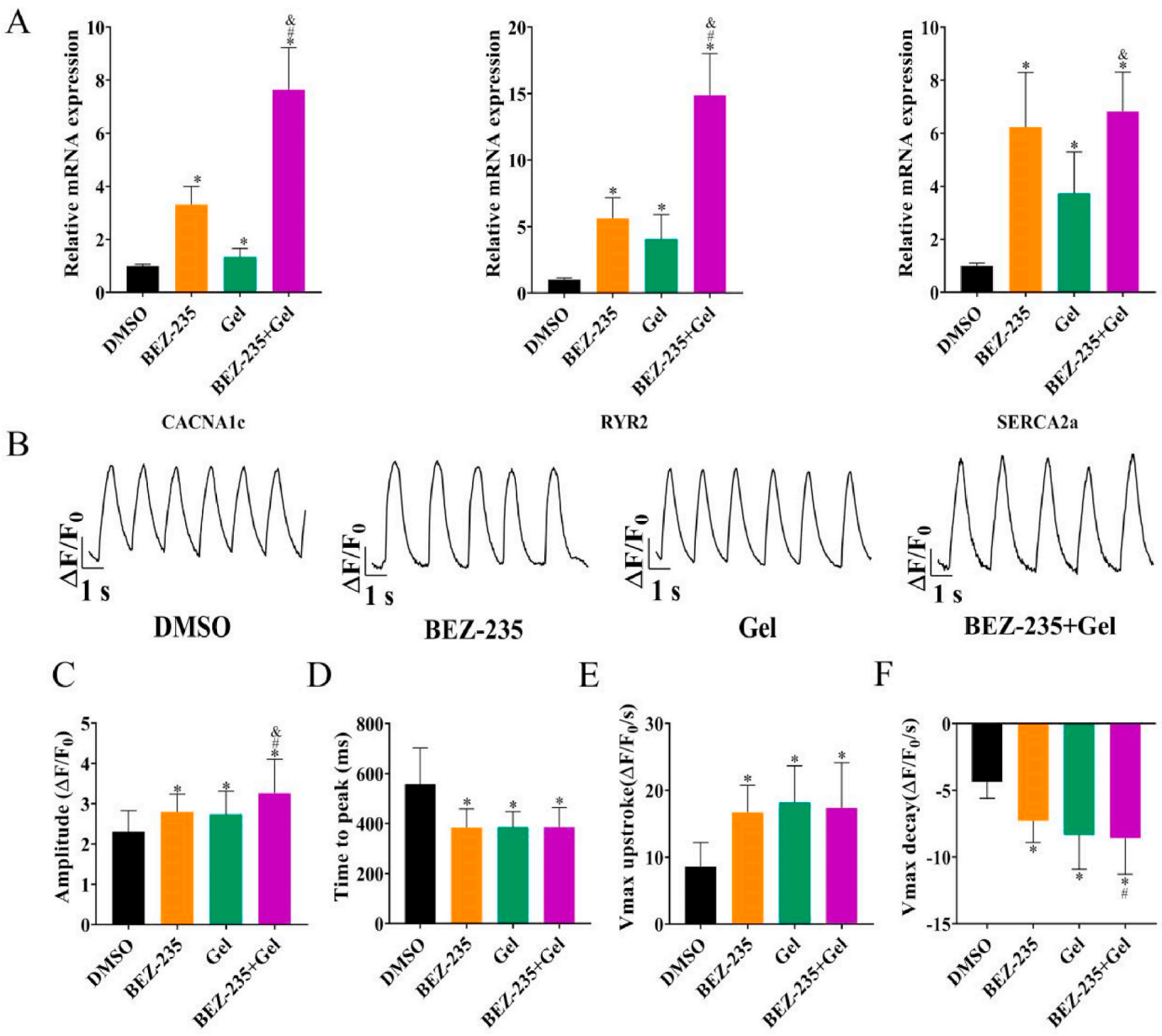

Fig. 7. BEZ-235 combined with Gel-treated iPSC-CMs exhibit improved calcium transient kinetics. (A) qRT-PCR analysis to examine the expressions of cardiac electrophysiological genes in iPSC-CMs. *P < 0.05 vs. DMSO, #P < 0.05 vs. BEZ-235, &P < 0.05 vs. Gel. n = 3. (B) Representative traces of calcium transients in each group. (C) Amplitude, (D) Time to peak, (E) V_{max} upstroke and (F) V_{max} decay. *P < 0.05 vs. DMSO, #P < 0.05 vs. BEZ-235, &P < 0.05 vs. Gel. n = 20–29 cells).

3.5. Effects of BEZ-235 + Gel on the microstructure of iPSC-CMs

We first analyzed the effect of different treatments on the sarcomere-related gene expression profiles of CMs (Fig. 5A). The expression of sarcomeric protein-encoding genes related to the maturation of CMs could be promoted to some extent by using the small molecule compound BEZ-235 or Gel alone. Importantly, the combination of the two above enhanced cTnT, troponinI 1 (TNNI 1), TNNI 3, myosin light chain (MYL2), MYL3, myosin heavy chain 6 (MYH 6) and MYH 7 expression levels more than monotherapy. We know that increased levels of TNNI 3 and MYH 7 also indicate more mature CMs [42,43]. As shown in Fig. S8A, the ratio of TNNI3/TNNI1 was highest in the BEZ-235 + Gel group. However, in the Gel or BEZ-235 + Gel groups, the magnitude of the increase in MYH7 was lower than that in MYH6 (Fig. S8B), and we speculate that this is related to our use of Gel as the medium for the growth of CMs, because the surface smoothness of Gel may not be comparable to that of culture plates, resulting in Some cells have insufficient extensibility.

Furthermore, adult CMs exhibit an elongated shape with organized myofibrils [44]. Immunoimages showed that iPSC-CMs in the untreated group were round and showed a shorter length, and after treatment with BEZ-235 or Gel, the cells showed a long spindle-shaped, more organized and arranged pattern with clear sarcomere streaks, and the cells appeared binuclear (Fig. 5B), the BEZ-235 + Gel group had the largest number of binucleated cells (Fig. S9A). The length of myofibrils or sarcomeres, as one of the indicators of maturation, is directly related to the contractility of cardiomyocytes [45]. In this study, iPSC-CMs had the longest sarcomere length (1.95 ± 0.17 μm) and aspect ratio (2.51 ± 0.75), and the lowest cell circularity index (0.43 ± 0.11) in the BEZ-235+Gel-treated group. Among them, iPSC-CMs treated with BEZ-235 combined with Gel were superior to Gel or BEZ-235 group in terms of sarcomere length, aspect ratio and circularity index. These results suggest that BEZ-235 + Gel drives iPSC-CMs toward maturation in multiple aspects, including cell morphology, sarcomere structure, ultrastructural changes, and gene expression (Fig. 5C–G).

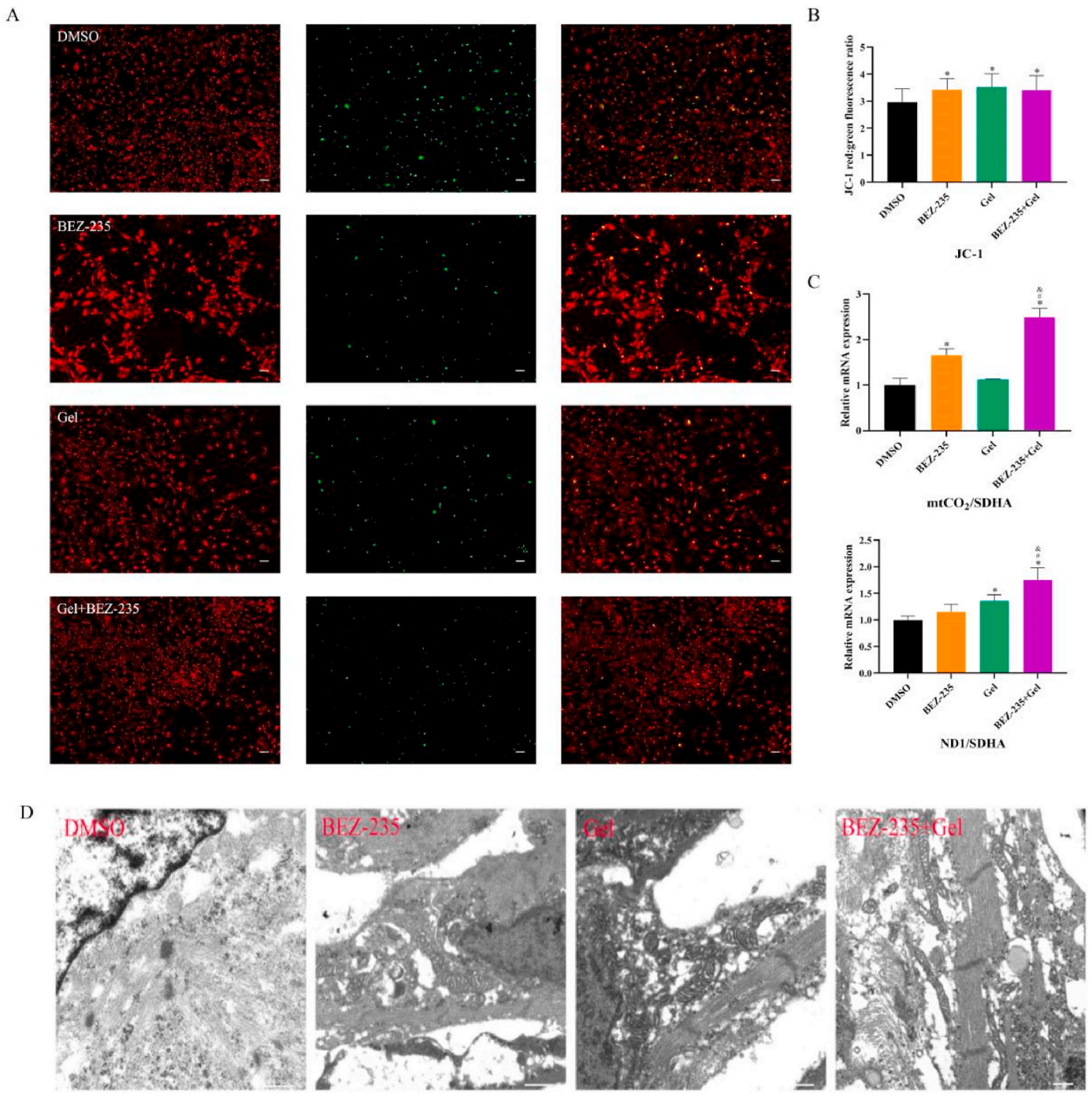

Fig. 8. Effects of BEZ-235 + Gel on mitochondrial membrane potential and mitochondrial morphology of iPSC-CMs. (A) Mitochondrial membrane potential analysis of iPSC-CMs in each group using fluorescent probe JC-1 assay system. Scale bar = 50 μm. (B) The ratio of red/green fluorescence in each group represents the level of ΔΨm. (C) Quantification of the ratio of mt-CO_2 or ND1 to SHDA DNA in each group. *P < 0.05 vs. DMSO, $^{\#}$P < 0.05 vs. BEZ-235, $^{\&}$P < 0.05 vs. Gel. n = 3. (D) Changes in the number and morphology of mitochondria observed by transmission electron microscopy (TEM). Scale bar = 500 nm.

3.6. Effects of BEZ-235 + Gel on the action potential of iPSC-CMs

The action potential of each CM is unique and controls the electrical behavior of CMs that are critical to cardiac function. Except for pacemaker cells, most adult CMs are quiescent and contract upon stimulation by pacemaker cells, whereas immature CMs exhibit spontaneous contractions due to the presence of distinct ion channels on the cells [17]. To further determine the maturity of the electrical properties of iPSC-CMs, we performed electrophysiological assessments (representative spontaneous action potential trajectories, Fig. 6A). It was found that the beat rate (BR) of iPSC-CMs treated with BEZ-235 was gradually slowed down compared with cells from DMSO (100.50 ± 25.93 vs. 152.80 ± 47.49 beat/min) (Fig. 6B), peak (51.51 ± 4.51 vs. 47.93 ± 4.79 mV) (Fig. 6C), action potential duration at 50% repolarization (APD50) (230.50 ± 64.56 vs. 155.30 ± 50.49 ms) (Fig. 6E), action potential duration at 90% repolarization (APD90) (271.40 ± 68.58 vs. 183.50 ± 58.71 ms) (Fig. 6F) increased. Although action potential amplitude (APA) (Fig. 6D) and APD50/90 (Fig. 6G) were not significantly improved, APA and APD50/90 were significantly increased when BEZ-235 was co-treated with Gel. More importantly, compared with the

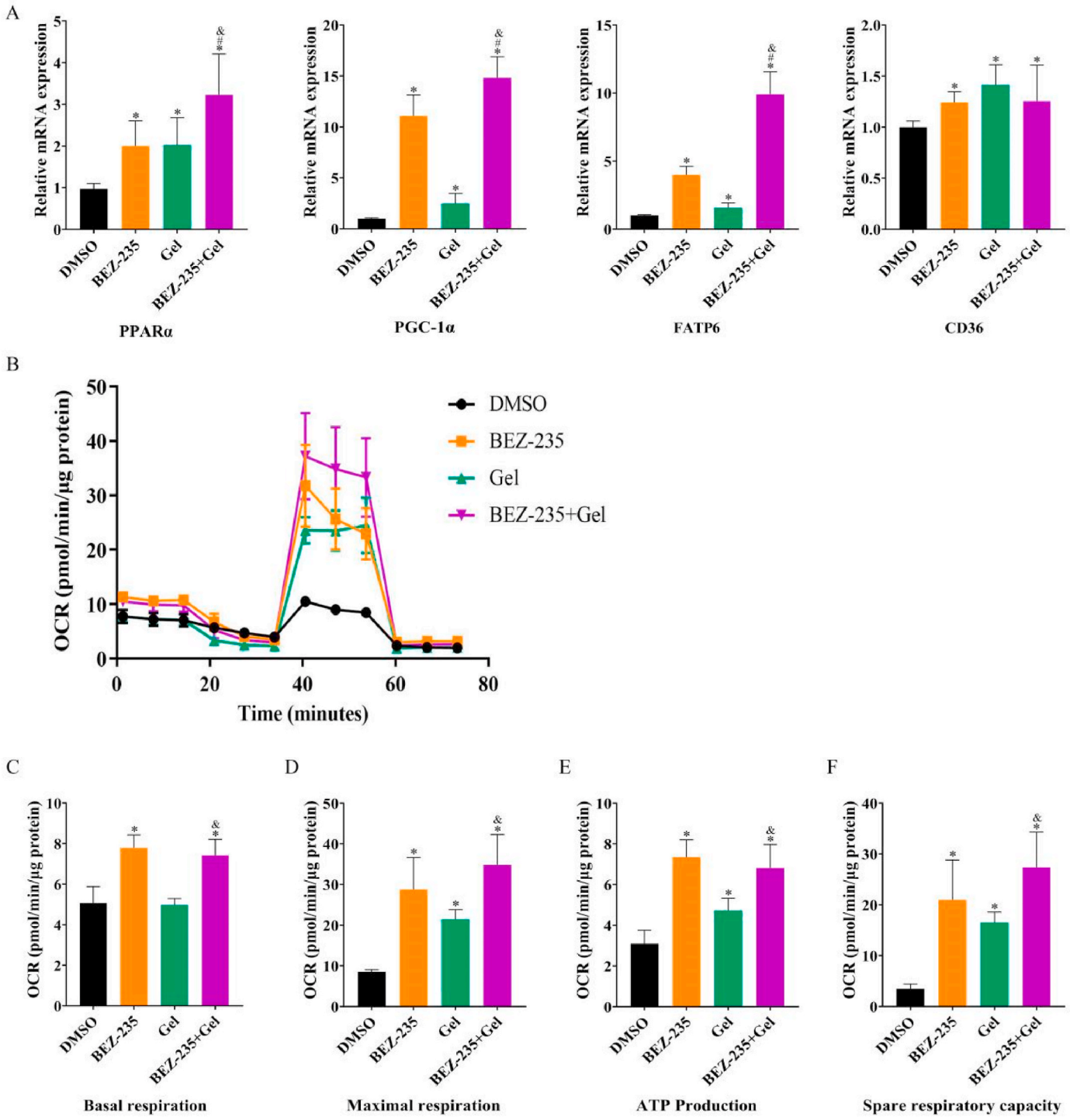

Fig. 9. The effect of BEZ-235 + Gel on metabolic function of iPSC-derived CMs. (A) Expression of genes related to metabolic function in iPSC-CMs after BEZ-235 and Gel treatment. *P < 0.05 vs. DMSO, #P < 0.05 vs. BEZ-235, &P < 0.05 vs. Gel. n = 3. (B) Representative traces showing the OCR of iPSC-CMs following sequential addition of oligomycin, FCCP, and rotenone/antimycin A. Quantification of basal respiration (C), maximal respiration (D), ATP production (E) and spare respiratory capacity (F). *P < 0.05 vs. DMSO, #P < 0.05 vs. BEZ-235, &P < 0.05 vs. Gel. n = 6.

BEZ-235 treatment group, BR (63.08 ± 18.89 beat/min) (Fig. 6B), APD50 (294.70 ± 65.05 ms) (Fig. 6E), APD90 (331.80 ± 65.39 ms) (Fig. 6F), APD50/90 (0.88 ± 0.03 ms) (Fig. 6G) of iPSC-CMs were more mature.

In addition, the electrical propagation and activity of CMs were assessed by measuring the surface potential on microelectrode arrays (MEA). The color map represents a snapshot of the electrical propagation in the monolayer, although the FPD gradually decreased in the BEZ-235 + Gel group (Fig. S9B), where the direction of the arrow indicates the direction of the local electrical propagation, indicating that iPSC-CMs produced more uniform electrical propagation due to BEZ-235 or Gel treatment (Fig. 6H).

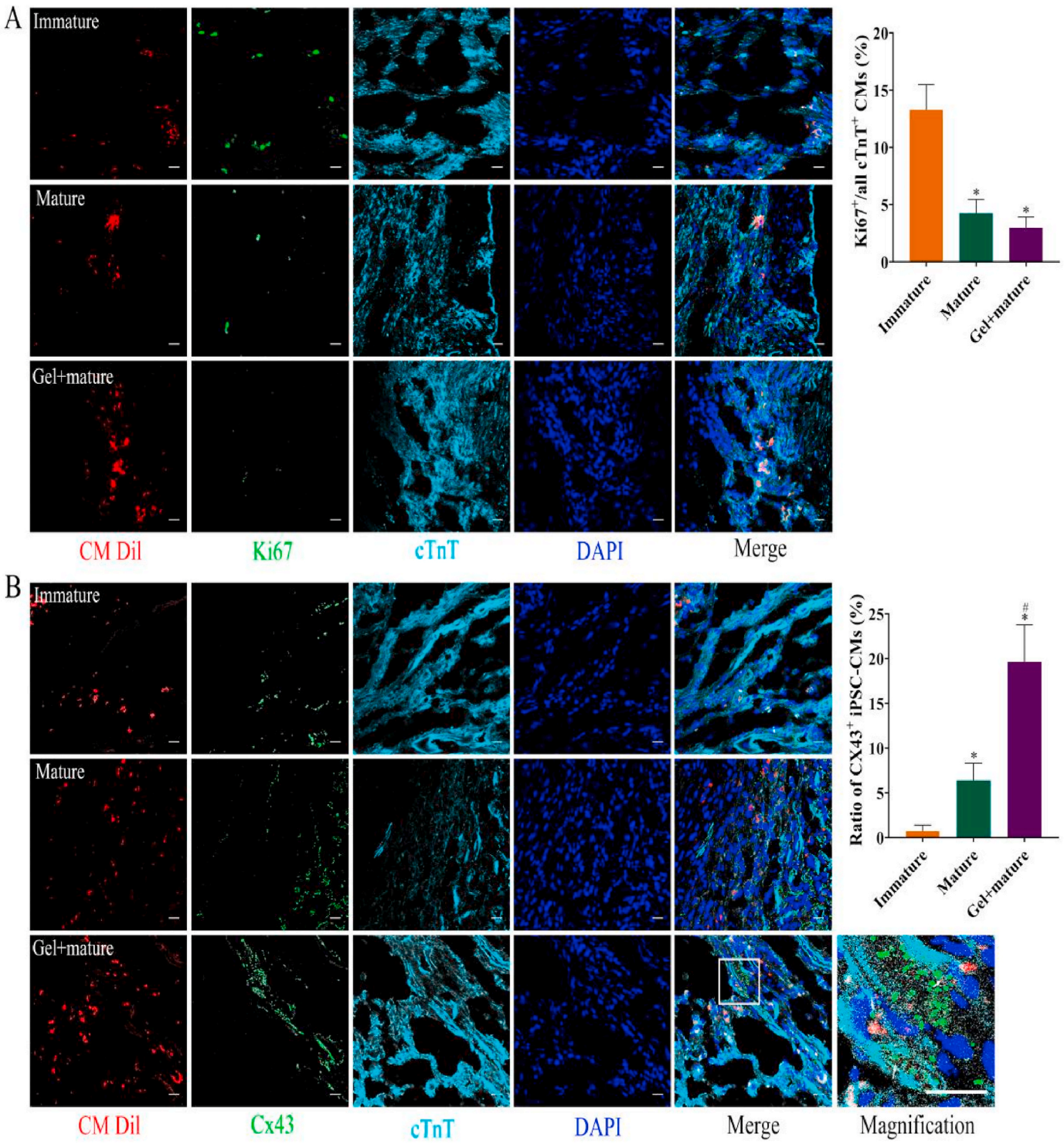

Fig. 10. Engraftment of mature and immature cardiomyocytes into infarcted mouse hearts. (**A**) Representative immunostaining showing Ki67$^+$ cells in cardiomyocyte grafts derived from immature and mature cells. (**B**) Effects of iPSC-CMs of different maturity on Cx43 expression. *P < 0.05 vs. Immature. $^{\#}$P < 0.05 vs. Mature. n = 3. Scale bar = 20μm.

3.7. Effects of BEZ-235 + Gel on calcium transients and conductance in iPSC-CMs

The second messenger Ca^{2+} plays a crucial role in cardiac electrical activity, it can directly activate myofilaments and cause contraction, and Ca^{2+} transients and various parameters are also indicators for evaluating the maturation of CMs [46]. Calcium voltage-gated channel subunit alpha 1 C (CACNA1C), cardiac ryanodine receptor (RYR2) and sarcoplasmic/endoplasmic reticulum Ca^{2+}ATPase 2a (SERCA2A) are genes related to CMs action potential and Ca^{2+} processing ability, which can reflect the electrophysiological maturity of cells [47]. BEZ-235 and Gel alone/co-intervention resulted in increased mRNA expression of CACNA1C, RYR2 and SERCA2A (Fig. 7A). To further investigate the maturation status of iPSC-CMs, we used Fluo-4 AM to indicate calcium handling of cells. Representative traces of Ca^{2+} influx are shown in Fig. 7B. After BEZ-235 combined with Gel treatment, the amplitude

(3.27 ± 0.83 vs. 2.31 ± 0.52ΔF/F_0) (Fig. 7C),V_{max} upstroke (17.35 ± 6.78 vs. 8.59 ± 3.61ΔF/F_0/s) (Fig. 7E) and V_{max} decay (−8.59 ± 2.70 vs. −4.38 ± 1.21ΔF/F_0/s) (Fig. 7F) of iPSC-CMs was significantly increased compared with DMSO group. Of these, the combined amplitude was greater than that of BEZ-235 alone (3.27 ± 0.83 vs. 2.80 ± 0.45ΔF/F0) or Gel (3.27 ± 0.83 vs. 2.74 ± 0.57ΔF/F0) (Fig. 7C). For Vmax decay, BEZ-235 + Gel was superior to BEZ-235 alone (−8.59 ± 2.70 vs. −7.27 ± 1.64ΔF/F0/s) treatment group (Fig. 7F). More importantly, whether BEZ-235 alone (384.34 ± 74.42 ms) or Gel (385.98 ± 61.37 ms), or both (386.25 ± 77.16 ms) treated iPSC-CMs, the time to peak $[Ca^{2+}]i$ was significantly shorter than that in the DMSO (558.28 ± 144.21 ms) group (Fig. 7D).

3.8. Effects of BEZ-235 + Gel on mitochondrial morphology and structure of iPSC-CMs

Mitochondrial bioenergetics and ATP production are key indicators of more mature CMs because mitochondrial function is highly increased in adult and mature CMs compared to neonatal and immature CMs [48,49]. To detect the differences in mitochondrial morphology of iPSC-CMs in different groups, the expression and morphological changes of mitochondrial production-related genes were compared among the four groups. We used the fluorescent probe JC-1 method to detect mitochondrial membrane potential (MMP), a key indicator of mitochondrial structural and functional integrity (Fig. 8A). The results showed that BEZ-235 + Gel treatment resulted in increased mitochondrial membrane potential in iPSC-CMs (Fig. 8B). Consistent with the above results, BEZ-235 combined with Gel significantly increased the ratio of mitochondria-encoded genes (Mitochondrial cytochrome oxidase II, mt-CO_2) and (NADH dehydrogenase subunit I, ND1) to nuclear DNA (Succinate dehydrogenase subunit A, SDHA) as detected by qRT-PCR. (Fig. 8C). Excitation-contraction coupling requires a large amount of energy, not only relying on a large number of mitochondria, but also its specific distribution in CMs [50]. By TEM, we found that the iPSC-CMs treated with BEZ-235 or Gel were different from the DMSO group. The number of mitochondria in the DMSO group was sparse, the shape was round, and the mitochondrial cristae were sparse, mostly distributed around the nucleus. In contrast, iPSC-CMs treated with BEZ-235 or Gel showed increased mitochondrial numbers, rod-like morphology, denser mitochondrial inner cristae matrix, and more concentrated distribution next to myofibrils (Fig. 8D). This structural change was also associated with an increase in mitochondrial oxidative capacity [51].

3.9. Effects of BEZ-235 + Gel on energy metabolism of iPSC-CMs

Peroxisome proliferator-activator receptor alpha (PPARα), a member of the ligand-activated nuclear transcription factor superfamily, can regulate myocardial energy metabolism at the gene expression level, affecting myocardial fatty acid and glucose metabolism [52]. In the Peroxisome proliferator-activated receptor gamma coactivator 1 (PGC-1) family, PGC-1α is a key regulator of mitochondrial biosynthesis and metabolism, and it is highly expressed in organs with high energy oxidative capacity, such as the heart [53]. Here, we observed that iPSC-CMs treated with BEZ-235 + Gel had 1.6-fold higher PPARα expression than those treated alone, and PGC-1α was 1.3-fold higher than BEZ-235 and 6-fold higher than Gel, respectively (Fig. 9A). The genes related to fatty acid oxidation, fatty acid transport protein 6 (FATP6) and cluster of differentiation 36 (CD36), were also significantly increased after BEZ-235 or Gel treatment. The expression of FATP6 after BEZ-235 + Gel treatment was 2.5 times and 6.2 times higher than that of BEZ-235 treatment, respectively (Fig. 9A).

To characterize mitochondrial function, we measured major aspects of mitochondrial coupling and respiratory control-basal respiration, maximal respiration, proton leak, non-mitochondrial respiration, and reserve capacity-using the Seahorse XF96 extracellular flux analyzer [51]. As expected, changes in OCR were detected after the sequential addition of the ATP synthase inhibitor oligomycin, the proton uncoupler FCCP, and the electron inhibitors rotenone and antimycin A. Fig. 9B shows representative traces of OCR of iPSC-CMs in each group. iPSC-CMs increased maximal respiration (Fig. 9D), ATP production (Fig. 9E) and residual respiration (Fig. 9F) after BEZ-235 or Gel treatment, with Gel + BEZ-235-treated cells having the highest maximal and residual respiration. It is worth noting that the basal respiration, maximal respiration, ATP production and residual respiration of iPSC-CMs treated with Gel + BEZ-235 were significantly higher than those of Gel alone group (Fig. 9C–F). The increase in the values of these major mitochondrial oxidation parameters indicated an enhanced mitochondrial oxidative capacity and also reflected the maturation of the metabolic function of iPSC-CMs [51].

3.10. Effects of gel on the retention rate of iPSC-CMs in the myocardium

To investigate the protective effect of Gel on cells, iPSC-CMs were labeled with CM Dil dye prior to intramyocardial in situ injection for in vivo tracking. 4 weeks after injection, tissue frozen sections were performed, and observed under a microscope, we found that after simple injection of iPSC-CMs, the retention rate of cells in the myocardium of mice was low, and the number of iPSC-CMs per high-power field was extremely sparse and scattered. In contrast, after injection of iPSC-CMs loaded with Gel, the number of intramyocardial cells was significantly increased, which was twice that of simple cell injection, and cell aggregation was observed (Fig. S10). This shows that Gel can significantly increase the survival rate of iPSC-CMs and prolong their action time in vivo. This may be related to the material itself, which can provide cells with an environment conducive to growth, and act as a delivery vehicle as a better physical barrier for cells. In conclusion, Gel can be used as a carrier medium for MI treatment in subsequent experiments.

3.11. Effects of Gel + mature on the formation of intramyocardial gap junctions

Since mature CMs are in a quiescent state, we next measured the proportion of $Ki67^+$ cells in different groups as an additional indicator of mature state [54]. The post-transplant Ki67 assay found that iPSC-CMs from mature had fewer proliferating cells than immature ones (Fig. 10A).

As the predominant connexin in CMs, Cx43 can cause electrical excitability and mechanical coupling between CMs [55]. It has been found that substantial defects in cell-cell coupling of immature PSC-CMs may be due to lower Cx43 membrane expression levels [56], which may also be responsible for arrhythmias following transplantation of immature CMs. We observed in the previous section by MEA that the electrical conductance of iPSC-CMs after maturation was more uniform and ordered, and the cellular conductance was closely related to the expression of Cx43. Therefore, in this part of the study, we investigated the expression of Cx43 in the myocardium of iPSC-CMs of different maturity by immunofluorescence staining of mouse myocardium. As shown in Fig. 10B, after transplantation of immature iPSC-CMs, it was difficult for cells to form gap junctions in the myocardium, and the expression of Cx43 was low. However, the formation of gap junctions in mature iPSC-CMs increased significantly after transplantation, which was 8.7 times that of immature cells. Whereas, in the case of Gel delivered as a vector, gap junction formation increased dramatically, 26-fold higher than in immature cells. In addition, the gap junctions formed by Gel + mature were also higher than those of the mature group ($P < 0.05$), and in addition to the formation of gap junctions between transplanted cells, it was also observed that some transplanted cells and mouse myocardium also formed gap junctions. From the above data, we know that mature iPSC-CMs can generate more gap junctions than immature cells, and these results are also consistent with previous studies [57]. After MI, improving intercellular signaling and promoting the formation of new blood vessels are the two most important aspects of improving prognosis

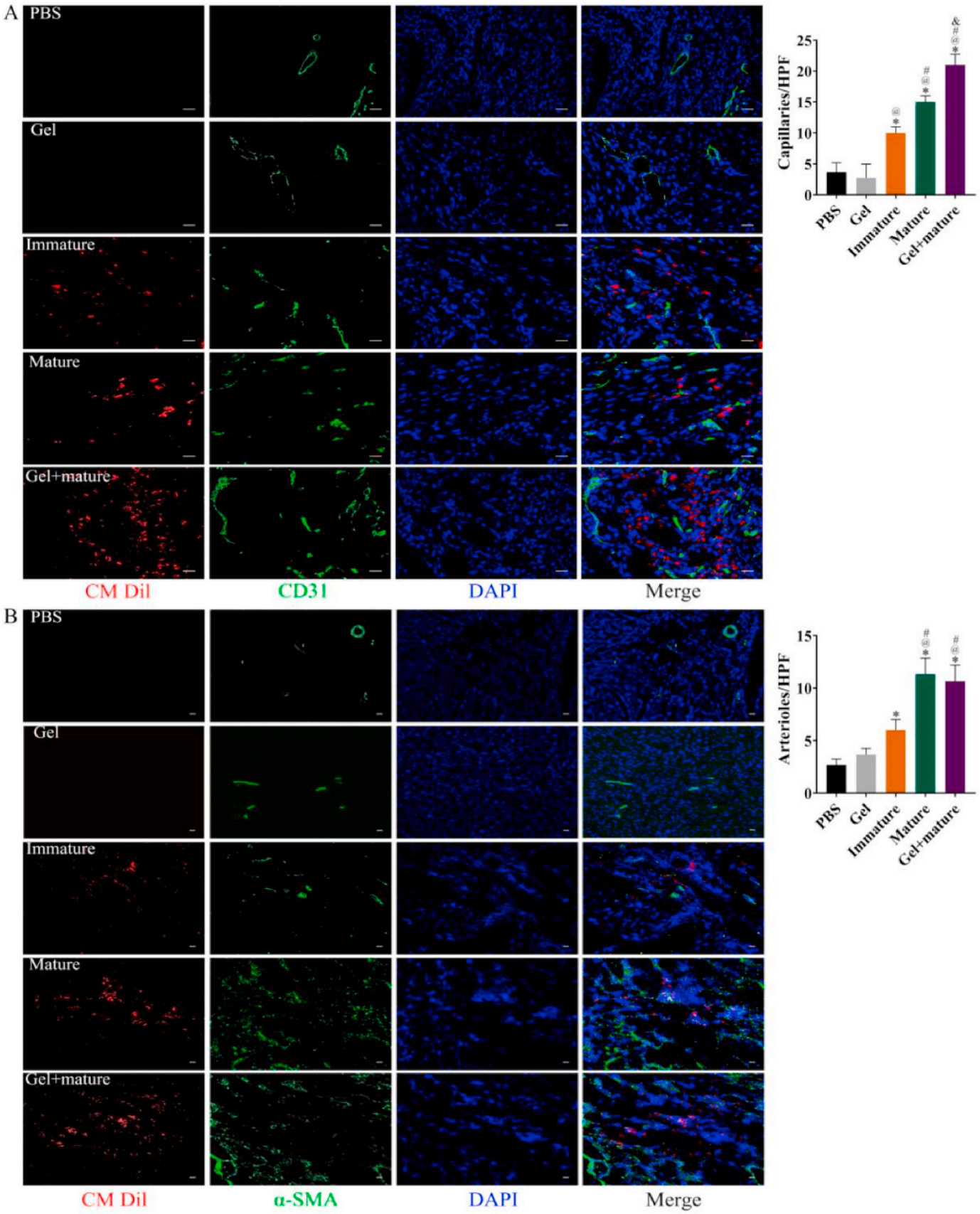

Fig. 11. Effects of iPSC-CMs of different maturity on angiogenesis. (A) Effects of iPSC-CMs of different maturity on CD31 expression. (B) Effects of iPSC-CMs of different maturity on α-SMA expression. *P < 0.05 vs. PBS. #P < 0.05 vs. Immature. &P < 0.05 vs. Mature. n = 3. Scale bar = 20μm.

[58]. In the case of Gel loading, the generated gap junction results are better than the transplantation of pure mature iPSC-CMs. We speculate that on the one hand, Gel may form a protective package for the cells to avoid direct exposure of the cells to the ischemic environment of MI, and on the other hand, it may be stimulated by the physical structure of Gel, which ultimately increases the formation of gap junctions.

3.12. Effects of Gel + mature on angiogenesis in MI mouse

A previous study demonstrated that the therapeutic effects of iPSC-CMs on damaged myocardium were partly attributable to their release of a broad spectrum of paracrine cytokines, including tumor necrosis factor-alpha, VEGF, interleukin-8, and granulocyte colony stimulation factor [59]. We assessed the level of capillary angiogenesis by iPSC-CMs of different maturation by staining mouse myocardium for CD31. Compared with the PBS group, the number of capillaries in the peripheral myocardial tissue of the immature iPSC-CMs after transplantation was significantly increased, and the number of blood vessels in the mature group was further increased compared with the immature group. After transplantation of Gel-loaded mature iPSC-CMs, the capillary angiogenesis effect was the highest among all groups and was more meaningful relative to transplantation of pure mature iPSC-CMs (Fig. 11A).

Next, we assessed the formation of different groups of arterioles by staining the mouse myocardium with α-SMA. The number of blood vessels in the peripheral myocardial tissue of immature iPSC-CMs after transplantation was increased compared with that in the PBS group, and the number of blood vessels in the mature group and Gel + mature group was further increased compared with the immature group (Fig. 11B). The above results indicate that mature iPSC-CMs can increase the number of blood vessels in the transplanted area more than immature, and the angiogenesis effect is better in the presence of Gel.

4. Conclusions

In summary, according to the composition of ECM, we synthesized a collagen-based soft matrix Gel, which has good biocompatibility and is suitable for cell growth. We combined the PI3K/AKT/mTOR pathway inhibitor BEZ-235 with Gel, which can better promote the maturation of iPSC-CMs in terms of structure, electrophysiology and metabolic function. Gel is also a good carrier for in vivo delivery of cells. Under the loading of Gel, it can prolong the retention rate of iPSC-CMs in the myocardium, and help mature iPSC-CMs to promote the expression of Cx43 and angiogenesis in the transplanted area. This also lays a good foundation for the subsequent treatment of mature iPSC-CMs.

Since transplanted cell survival is inversely proportional to maturation state, cell cycle activity and ischemia resistance decline as CM matures. For more mature iPSC-CMs, possibly mediating the recovery of cardiac function in vivo is not its therapeutic advantage. Therefore, at present, the application of more mature iPSC-CMs mainly focuses on the degree of electrophysiological integration after transplantation. Therefore, in follow-up studies, whether it is possible to find a critical point for iPSC-CMs to have both the treatment of myocardial infarction and the integration of electrophysiology, we think this may be an encouraging thing.

CRediT authorship contribution statement

Peng Wu: Conceptualization, Methodology, Software, Writing – review & editing. **Xiyalatu Sai:** Conceptualization, Methodology, Software. **Zhetao Li:** Data curation, Writing – original draft. **Xing Ye:** Data curation, Writing – original draft. **Li Jin:** Visualization, Investigation. **Guihuan Liu:** Supervision. **Ge Li:** Software, Validation. **Pingzhen Yang:** Data curation. **Mingyi Zhao:** Data curation, Writing – original draft. **Shuoji Zhu:** Data curation, Writing – original draft. **Nanbo Liu:** Data curation, Writing – original draft. **Ping Zhu:** Conceptualization, Methodology, Software, Writing – review & editing.

Declaration of competing interest

The authors declare no competing financial interest.

Acknowledgements

This research was funded by National Key Research and Development Program of China (2018YFA0108700,2017YFA0105602), NSFC Projects of INTERNATIONAL COOPERATION and Exchanges (81720108004), National Natural Science Foundation of China (81974019), The Research Team Project of Natural Science Foundation of Guangdong Province of China (2017A030312007). Science and Technology Planning Project of Guangdong Province (2022B1212010010),The key program of guangzhou science research plan (201904020047). The Special Project of Dengfeng Program of Guangdong Provincial People's Hospital (DFJH201812; KJ012019119; KJ012019423). The National Natural Science Foundation of China (82001301); and the Special Project of Dengfeng Program of Guangdong Provincial People's Hospital (KY0120220133, DFJHBF202111, KJ012020630).

Appendix A. Supplementary data

Supplementary data to this article can be found online at https://doi.org/10.1016/j.bioactmat.2022.05.024.

References

[1] Z. Chen, C.Y. Zeng, W.E. Wang, Progress of stem cell transplantation for treating myocardial infarction, Curr. Stem Cell Res. Ther. 12 (8) (2017) 624–636.
[2] K. Takahashi, S. Yamanaka, Induction of pluripotent stem cells from mouse embryonic and adult fibroblast cultures by defined factors, Cell 126 (4) 2006 663-676.
[3] K. Takahashi, K. Tanabe, M. Ohnuki, M. Narita, T. Ichisaka, K. Tomoda, S. Yamanaka, Induction of pluripotent stem cells from adult human fibroblasts by defined factors, Cell 131 (5) (2007) 861–872.
[4] J.Y. Yu, M.A. Vodyanik, K. Smuga-Otto, J. Antosiewicz-Bourget, J.L. Frane, S. L. Tian, J. Nie, G.A. Jonsdottir, V. Ruotti, R. Stewart, I.I. Slukvin, J.A. Thomson, Induced pluripotent stem cell lines derived from human somatic cells, Science 318 (5858) (2007) 1917–1920.
[5] N. Daniele, M. Campus, C. Pellegrini, E. Shkëmbi, F. Zinno, Biobanks and clinical research: an "interesting'' connection, Peertechz J Cytol Pathol 1 (2016), 034-043.
[6] A. Ntai, S. Baronchelli, S.A. La, A. Moles, A. Guffanti, B.P. De, I. Biunno, A review of research-grade human induced pluripotent stem cells qualification and biobanking processes, Biopreserv. Biobanking 15 (4) (2017) 384–392.
[7] Hadassah medical organization development of iPS from donated somatic cells of patients with neurological diseases. ClinicalTrials.gov identifier: NCT00874783. [(accessed on 10 may 2021)]; derivation of induced pluripotent stem cells from somatic cells donated by patients with neurological diseases for the study of the pathogenesis of the disorders and development of novel therapies. Available online: https://clinicaltrials.gov/ct2/show/NCT00874783.
[8] Sun X. Thalassemia Treatment Based on the Stem Cell Technology. ClinicalTrials.gov Identifier: NCT03222453. [(accessed on 10 May 2021)]; Available online: https://clinicaltrials.gov/ct2/show/NCT03222453..
[9] Memorial Sloan Kettering Cancer Center Generation of Heart Muscle Cells from Blood or Skin Cells of Breast Cancer Patients. ClinicalTrials.gov Identifier: NCT02772367. [(accessed on 10 May 2021)]; Generation of Induced Pluripotent Stem Cell Derived Cardiomyocytes from Patients Exposed to Trastuzumab Therapy for Breast Cancer. Available online: https://clinicaltrials.gov/ct2/show/NCT02772367.
[10] Moorfields Eye Hospital NHS Foundation Trust A Study Of Implantation Of Retinal Pigment Epithelium in Subjects with Acute Wet Age Related Macular Degeneration. ClinicalTrials.gov Identifier: NCT01691261. [(accessed on 10 May 2021)]; Phase 1, Open-Label, Safety and Feasibility Study of Implantation of PF-05206388 (Human Embryonic Stem Cell Derived Retinal Pigment Epithelium (RPE) Living Tissue Equivalent) in Subjects with Acute Wet Age Related Macular Degeneration and Recent Rapid Vision Decline. Available online: https://clinicaltrials.gov/ct2/show/NCT01691261..
[11] K.K. Hirschi, S. Li, K. Roy, Induced pluripotent stem cells for regenerative medicine, Annu. Rev. Biomed. Eng. 16 (2014) 277–294.
[12] X.M. Guan, W.Z. Xu, H. Zhang, Q. Wang, J.Y. Yu, R.Y. Zhang, Y.M. Chen, Y.L. Xia, J.X. Wang, D.J. Wang, Transplantation of human induced pluripotent stem cell-derived cardiomyocytes improves myocardial function and reverses ventricular remodeling in infarcted rat hearts, Stem Cell Res. Ther. 11 (1) (2020) 73.
[13] R. Romagnuolo, H. Masoudpour, A. Porta-Sánchez, B.P. Qiang, J. Barry, A. Laskary, X.L. Qi, S. Massé, K. Magtibay, H. Kawajiri, J. Wu, S.T. Valdman, J. Rothberg, K.M. Panchalingam, E. Titus, R.K. Li, P.W. Zandstra, G.A. Wright,

K. Nanthakumar, N.R. Ghugre, G. Keller, M.A. Laflamme, Human embryonic stem cell-derived cardiomyocytes regenerate the infarcted pig heart but induce ventricular tachyarrhythmias, Stem Cell Rep. 12 (5) (2019) 967–981.
[14] T. Kamakura, T. Makiyama, K. Sasaki, Y. Yoshida, Y. Wuriyanghai, J.R. Chen, T. Hattori, S. Ohno, T. Kita, M. Horie, S. Yamanaka, T. Kimura, Ultrastructural maturation of human-induced pluripotent stem cell-derived cardiomyocytes in a long-term culture, Circ. J. 77 (5) (2013) 1307–1314.
[15] X.L. Yang, M. Rodriguez, L. Pabon, K.A. Fischer, H. Reinecke, M. Regnier, N. J. Sniadecki, H. Ruohola-Baker, C.E. Murry, Tri-iodo-l-thyronine promotes the maturation of human cardiomyocytes-derived from induced pluripotent stem cells, J. Mol. Cell. Cardiol. 72 (2014) 296–304.
[16] S.S. Parikh, D.J. Blackwell, N. Gomez-Hurtado, M. Frisk, L.L. Wang, K. Kim, C. P. Dahl, A. Fiane, T. Tønnessen, D.O. Kryshtal, W.E. Louch, B.C. Knollmann, Thyroid and glucocorticoid hormones promote functional T-tubule development in human-induced pluripotent stem cell-derived cardiomyocytes, Circ. Res. 121 (12) (2017) 1323–1330.
[17] Y. Horikoshi, Y.S. Yan, M. Terashvili, C. Wells, H. Horikoshi, S. Fujita, Z.J. Bosnjak, X.W. Bai, Fatty acid-treated induced pluripotent stem cell-derived human cardiomyocytes exhibit adult cardiomyocyte-like energy metabolism phenotypes, Cells 8 (9) (2019). https://doi:10.3390/cells8091095.
[18] X.L. Yang, M.L. Rodriguez, A. Leonard, L.H. Sun, K.A. Fischer, Y.L. Wang, J. Ritterhoff, L.M. Zhao, S.C. Kolwicz, L. Pabon, H. Reinecke, N.J. Sniadecki, R. Tian, H. Ruohola-Baker, H.D. Xu, C.E. Murry, Fatty acids enhance the maturation of cardiomyocytes derived from human pluripotent stem cells, Stem Cell Rep. 13 (4) (2019) 657–668.
[19] R.A. Lasher, A.Q. Pahnke, J.M. Johnson, F.B. Sachse, R.W. Hitchcock, Electrical stimulation directs engineered cardiac tissue to an age-matched native phenotype, J. Tissue Eng. 3 (1) (2012), 2041731412455354.
[20] S.S. Nunes, J.W. Miklas, J. Liu, R. Aschar-Sobbi, Y. Xiao, B.Y. Zhang, J.H. Jiang, S. Massé, M. Gagliardi, A. Hsieh, N. Thavandiran, M.A. Laflamme, K. Nanthakumar, G.J. Gross, P.H. Backx, G. Keller, M. Radisic, Biowire: a platform for maturation of human pluripotent stem cell-derived cardiomyocytes, Nat. Methods 10 (8) (2013) 781–787.
[21] L.J. Fu, W. Wu, X.J. Sun, P. Zhang, Glucocorticoids enhanced osteoclast autophagy through the PI3K/Akt/mTOR signaling pathway, Calcif. Tissue Int. 107 (1) (2020) 60–71.
[22] L. Sun-Hee, J. Jun-Goo, B. Jong-Sup, L. Kwang-Hyoen, Y.M. Lee, A group of novel HIF-1α inhibitors, glyceollins, blocks HIF-1α synthesis and decreases its stability via inhibition of the PI3K/AKT/mTOR pathway and Hsp 90 binding, J. Cell. Physiol. 230 (4) (2015) 853–862.
[23] H. Nakano, I. Minami, D. Braas, H. Pappoe, X.J. Wu, A. Sagadevan, L. Vergnes, K. Fu, M. Morselli, C. Dunham, X.Q. Ding, A.Z. Stieg, J.K. Gimzewski, M. Pellegrini, P.M. Clark, K. Reue, A.J. Lusis, B. Ribalet, S.K. Kurdistani, H. Christofk, N. Nakatsuji, A. Nakano, Glucose inhibits cardiac muscle maturation through nucleotide biosynthesis, Elife 6 (2017), https://doi.org/10.7554/eLife.29330.
[24] K.T. Kuppusamy, D.C. Jones, H. Sperber, A. Madan, K.A. Fischer, M.L. Rodriguez, L. Pabon, W.Z. Zhu, N.L. Tulloch, X.L. Yang, N.J. Sniadecki, M.A. Laflamme, W. L. Ruzzo, C.E. Murry, H. Ruohola-Baker, Let-7 family of microRNA is required for maturation and adult-like metabolism in stem cell-derived cardiomyocytes, Proc. Natl. Acad. Sci. U. S. A. 112 (21) (2015) E2785–E2794.
[25] C. Correia, A. Koshkin, P. Duarte, D.J. Hu, A. Teixeira, I. Domian, M. Serra, P. M. Alves, Distinct carbon sources affect structural and functional maturation of cardiomyocytes derived from human pluripotent stem cells, Sci. Rep. 7 (1) (2017) 8590.
[26] J.C. Garbern, A. Helman, R. Sereda, M. Sarikhani, A. Ahmed, G.O. Escalante, R. Ogurlu, S.L. Kim, J.F. Zimmerman, A. Cho, L. MacQueen, V.J. Bezzerides, K. K. Parker, D.A. Melton, R.T. Lee, Inhibition of mTOR signaling enhances maturation of cardiomyocytes derived from human-induced pluripotent stem cells via p53-induced quiescence, Circulation 141 (4) (2020) 285–300.
[27] T. Rozario, D.W. DeSimone, The extracellular matrix in development and morphogenesis: a dynamic view, Dev. Biol. 341 (1) (2010) 126–140.
[28] N. Bildyug, Extracellular matrix in regulation of contractile system in cardiomyocytes, Int. J. Mol. Sci. 20 (20) (2019) 5054.
[29] N.B. Bil'diug, N.M. Iudintseva, G.P. Pinaev, Contractile apparatus organization of cardiomyocytes upon their cultivation in collagen gels, Tsitologiia 56 (11) (2014) 822–827.
[30] D.M. Lyra-Leite, A.M. Andres, A.P. Petersen, N.R. Ariyasinghe, N. Cho, J.A. Lee, R. A. Gottlieb, M.L. McCain, Mitochondrial function in engineered cardiac tissues is regulated by extracellular matrix elasticity and tissue alignment, Am. J. Physiol. Heart Circ. Physiol. 313 (4) (2017) H757–H767.
[31] C.C. Veerman, G. Kosmidis, C.L. Mummery, S. Casini, A.O. Verkerk, M. Bellin, Immaturity of human stem-cell-derived cardiomyocytes in culture: fatal flaw or soluble problem? Stem Cell. Dev. 24 (9) (2015) 1035–1052.
[32] S. Lee, V. Serpooshan, X.M. Tong, S. Venkatraman, M. Lee, J. Lee, O. Chirikian, J. C. Wu, S.M. Wu, F. Yang, Contractile force generation by 3D hiPSC-derived cardiac tissues is enhanced by rapid establishment of cellular interconnection in matrix with muscle-mimicking stiffness, Biomaterials 131 (2017) 111–120.
[33] G. Forte, S. Pagliari, M. Ebara, K. Uto, J. Tam, S. Romanazzo, C. Escobedo-Lucea, E. Romano, N.P. Di, E. Traversa, T. Aoyagi, Substrate stiffness modulates gene expression and phenotype in neonatal cardiomyocytes in vitro, Tissue Eng. 18 (2012) 1837–1848.
[34] T.j. Herron, A. Rocha, K.F. Campbell, D. Ponce-Balbuena, B.C. Willis, G. Guerrero-Serna, Q.H. Liu, M. Klos, H. Musa, M. Zarzoso, A. Bizy, J. Furness, J. Anumonwo, S. Mironov, J. Jalife, Extracellular matrix-mediated maturation of human pluripotent stem cell-derived cardiac monolayer structure and electrophysiological function, Circ Arrhythm Electrophysiol 9 (4) (2016), e003638.
[35] R. Bao, B.Y. Tan, S. Liang, N. Zhang, W. Wang, W.G. Liu, A π-π conjugation-containing soft and conductive injectable polymer hydrogel highly efficiently rebuilds cardiac function after myocardial infarction, Biomaterials 122 (2017) 63–71.
[36] P.W. Burridge, E. Matsa, P. Shukla, Z.C. Lin, J.M. Churko, A.D. Ebert, F. Lan, S. Diecke, B. Huber, N.M. Mordwinkin, J.R. Plews, O.J. Abilez, B.X. Cui, J.D. Gold, J. C. Wu, Chemically defined generation of human cardiomyocytes, Nat. Methods. 11 (8) (2014) 855-860.lian xiaojun., bao xiaoping., zilberter misha., westman mattias., Fisahn andré., hsiao Cheston., hazeltine Laurie B., dunn Kaitlin K., Kamp timothy J., palecek sean P.(2015). chemically defined, albumin-free human cardiomyocyte generation. Nat Methods, 12(7), 595-860. doi:10.1038/nmeth.3448.
[37] C. Cui, L. Geng, J. Shi, Y. Zhu, G. Yang, Z. Wang, J. Wang, M. Chen, Structural and electrophysiological dysfunctions due to increased endoplasmic reticulum stress in a long-term pacing model using human induced pluripotent stem cell-derived ventricular cardiomyocytes, Stem Cell Res. Ther. 8 (1) (2017) 109.
[38] L. Goldbloom-Helzner, D.K. Hao, A. Wang, Developing regenerative treatments for developmental defects, injuries, and diseases using extracellular matrix collagen-targeting peptides, Int. J. Mol. Sci. 20 (17) (2019). https://doi:10.3390/ijms20174072.
[39] R. Hesselbarth, T.U. Esser, K. Roshanbinfar, S. Schrüfer, D.W. Schubert, F.B. Engel, CHIR99021 promotes hiPSC-derived cardiomyocyte proliferation in engineered 3D microtissues, Adv Healthc Mater 10 (20) (2021), e2100926.
[40] J.N. Tang, J.Q. Wang, K. Huang, Y.Q. Ye, T. Su, L. Qiao, M.T. Hensley, T. G. Caranasos, J.Y. Zhang, Z. Gu, K. Cheng, Cardiac cell-integrated microneedle patch for treating myocardial infarction, Sci. Adv. 4 (11) (2018), eaat9365.
[41] D.Y. Lü, C.H. Luo, C. Zhang, Z. Li, M. Long, Differential regulation of morphology and stemness of mouse embryonic stem cells by substrate stiffness and topography, Biomaterials 35 (13) (2014) 3945–3955.
[42] F.B. Bedada, S.S.K. Chan, S.K. Metzger, L.Y. Zhang, J.Y. Zhang, D.J. Garry, T. J. Kamp, M. Kyba, J.M. Metzger, Acquisition of a quantitative, Stoichiometrically Conserved Ratiometric marker of maturation status in stem cell-derived cardiac myocytes, Stem Cell Rep. 3 (2014) 594–605.
[43] S. Yoshida, S. Miyagawa, S. Fukushima, T. Kawamura, N. Kashiyama, F. Ohashi, T. Toyofuku, K. Toda, Y. Sawa, Maturation of human induced pluripotent stem cell-derived cardiomyocytes by soluble factors from human mesenchymal stem cells, Mol. Ther. 26 (2018) 2681–2695.
[44] A.M. Gerdes, S.E. Kellerman, J.A. Moore, K.E. Muffly, L.C. Clark, P.Y. Reaves, K. B. Malec, P.P. McKeown, D.D. Schocken, Structural remodeling of cardiac myocytes in patients with ischemic cardiomyopathy, Circulation 86 (1992) 426–430.
[45] J.C. Kentish, H.E. ter Keurs, L. Ricciardi, J.J. Bucx, M.I. Noble, Comparison between the sarcomere length-force relations of intact and skinned trabeculae from rat right ventricle. Influence of calcium concentrations on these relations, Circ. Res. 58 (6) (1986) 755–768.
[46] G. Chen, S. Li, I. Karakikes, L. Ren, C.M. Zi-Ying, A. Chopra, W. Keung, B. Yan, C.W. Y. Chan, K.D. Costa, C.W. Kong, R.J. Hajjar, C.S. Chen, R.A. Li, Phospholamban as a crucial determinant of the inotropic response of human pluripotent stem cell derived ventricular cardiomyocytes and engineered 3-dimensional tissue constructs, Circ, Arrhythmia Electrophysiol 8 (2015) 193–202.
[47] C. Cui, J.X. Wang, D.D. Qian, J.Y. Huang, J. Lin, P. Kingshott, P.Y. Wang, M. L. Chen, Binary colloidal Crystals drive Spheroid formation and accelerate maturation of human-induced pluripotent stem cell-derived cardiomyocytes, ACS Appl. Mater. Interfaces 11 (4) (2019) 3679–3689.
[48] X.L. Yang, L. Pabon, C.E. Murry, Engineering adolescence: maturation of human pluripotent stem cell-derived cardiomyocytes, Circ. Res. 114 (2014) 511–523.
[49] K. Ronaldson-Bouchard, S.P. Ma, K. Yeager, T. Chen, L.J. Song, D. Sirabella, K. Morikawa, D. Teles, M. Yazawa, G. Vunjak-Novakovic, Advanced maturation of human cardiac tissue grown from pluripotent stem cells, Nature 556 (7700) (2019) 239–243.
[50] C.L. Hoppel, B. Tandler, H. Fujioka, A. Riva, Dynamic organization of mitochondria in human heart and in myocardial disease, Int. J. Biochem. Cell Biol. 41 (10) (2019) 1949–1956.
[51] C. Gentillon, D. Li, M.X. Duan, W.M. Yu, M.K. Preininger, R. Jha, A. Rampoldi, A. Saraf, G.C. Gibson, C.K. Qu, L.A. Brown, C.H. Xu, Targeting HIF-1α in combination with PPARα activation and postnatal factors promotes the metabolic maturation of human induced pluripotent stem cell-derived cardiomyocytes, J. Mol. Cell. Cardiol.. 132 (139), 120-135.
[52] S. Chung, P.P. Dzeja, R.S. Faustino, C. Perez-Terzic, A. Behfar, A. Terzic, Mitochondrial oxidative metabolism is required for the cardiac differentiation of stem cells, Nat. Clin. Pract. Cardiovasc. Med. 4 (Suppl. 1) (2007) S60–S67.
[53] G.C. Rowe, A. Jiang, Z. Arany, PGC-1 coactivators in cardiac development and disease, Circ. Res. 107 (7) (2010) 825–838.
[54] S. Funakoshi, I. Fernandes, O. Mastikhina, D. Wilkinson, T. Tran, W. Dhahri, A. Mazine, D.H. Yang, B. Burnett, J. Lee, S. Protze, G.D. Bader, S.S. Nunes, M. Laflamme, G. Keller, Generation of mature compact ventricular cardiomyocytes from human pluripotent stem cells, Nat. Commun. 12 (1) (2021) 3155.
[55] I. Epifantseva, R.M. Shaw, Intracellular trafficking pathways of Cx43 gap junction channels, Biochim. Biophys. Acta Biomembr. 1860 (1) (2018) 40–47.
[56] R.R. Besser, M. Ishahak, V. Mayo, D. Carbonero, I. Claure, A. Agarwal, Engineered microenvironments for maturation of stem cell derived cardiac myocytes, Theranostics 8 (1) (2018) 124–140.
[57] W. Dhahri, V.T. Sadikov, D. Wilkinson, E. Pereira, E. Ceylan, N. Andharia, B. P. Qiang, H. Masoudpour, F. Wulkan, E. Quesnel, W.L. Jiang, S. Funakoshi, A. Mazine, M.J. Gomez-Garcia, N Latifi, Y.D. Jiang, E. Huszti, C.A. Simmons, G. Keller, M.A. Laflamme, In Vitro Matured Human Pluripotent Stem Cell-derived

Cardiomyocytes Form Grafts With Enhanced Structure and Function in Injured Hearts, Circulation 145 (18) (2022) 1412–1426.
[58] X.J. Wei, S. Chen, T. Xie, H.C. Chen, X. Jin, J.M. Yang, S. Sahar, H.L. Huang, S. J. Zhu, N.B. Liu, C.J. Yu, P. Zhu, W. Wang, W. Zhang, An MMP-degradable and conductive hydrogel to stabilize HIF-1α for recovering cardiac functions, Theranostics 12 (1) (2022) 127–142.
[59] A. Tachibana, M.R. Santoso, M. Mahmoudi, P. Shukla, L. Wang, M. Bennett, A. B. Goldstone, M. Wang, M. Fukushi, A.D. Ebert, Y.J. Woo, E. Rulifson, P.C. Yang, Paracrine effects of the pluripotent stem cell-derived cardiac myocytes Salvage the injured myocardium, Circ. Res. 121 (6) (2017) e22–e36.

Glossary

iPSCs: Induced pluripotent stem cells
iPSC-CMs: Induced pluripotent stem cell-derived cardiomyocytes
MI: Myocardial infarction
Gel: Nano colloidal gelatin